Annual crops buffer, irrigation infrastructure does not: crop composition and WUE drought sensitivity in Chile

(This paper is a non-peer reviewed preprint submitted to EarthArXiv)

Francisco Zambrano[a,*], Francisco Fernández[b], María Molinos-Senante[c]

[a] *Facultad de Medicina Veterinaría y Agronomía, Universidad de Las Américas, Chile,*

[b] *Facultad de Economía, Negocios y Gobierno, Universidad San Sebastián, Santiago, Chile,*

[c] *Institute of Sustainable Processes, Universidad de Valladolid, Valladolid, Spain, 47011*

Abstract

Agricultural water use efficiency (WUE) is widely expected to improve under technological intensification, yet its response to prolonged aridification at regional scales is poorly understood. We analyzed spatiotemporal patterns of WUE across 127 Chilean agricultural sub-watersheds from 2001 to 2020, a period spanning an unprecedented megadrought. WUE responses were spatially heterogeneous: arid and semi-arid sub-watersheds showed predominantly negative ΔWUE, while irrigated Mediterranean sub-watersheds showed positive ΔWUE; negative long-term trends and structural breaks concentrated in the 30-35°S band. Precipitation deficit indices dominated cross-sectional WUE sensitivity; at the 36-month accumulation scale, SPEI and SPI showed practically equivalent explanatory power (TOST $p < 0.001$, 90% CI [−0.004, +0.003]).

Crop system composition is associated with WUE drought sensitivity through two contrasting patterns, each constrained by a different form of confounding. Annual-crop prevalence is robustly and negatively associated with drought sensitivity across all latitude specifications (SEM $\beta = -0.322$ to -0.485, $p < 0.01$); whether this reflects structural buffering or drought-driven reduction of annual cultivation cannot be established from the observational data alone. Irrigation infrastructure prevalence is positively associated with WUE-drought coupling in the full sample (SEM $\beta = +0.422$, $p < 0.001$), but this association attenuates to non-significance when latitude is explicitly controlled ($\beta = +0.109$, $p = 0.327$) and cannot be statistically isolated from the latitudinal aridity gradient; within the warm-summer-Mediterranean zone the association is marginal ($\beta = +0.264$, $p = 0.053$). Both patterns are associative; causal inference is not possible given the observational design and spatial confounding.

These patterns are consistent with crop-portfolio flexibility reducing structural drought exposure under

prolonged aridification, and with WUE-based efficiency metrics being insufficient indicators of agricultural resilience where irrigation supply is hydrologically coupled to the same signals that suppress crop productivity. These findings have implications for water governance and agricultural planning in snowmelt-dependent dryland regions globally.

Keywords: water use efficiency, megadrought, aridification, SPEI, Chile, NPP/ET, crop composition

1. Introduction

Global agriculture consumes approximately 70% of freshwater withdrawals (Hoekstra and Mekonnen, 2012), yet whether irrigation infrastructure buffers or amplifies agricultural water use efficiency (WUE) sensitivity under prolonged drought remains poorly understood. The widely held assumption that irrigation protects crop production from meteorological variability has been challenged on two fronts. The irrigation efficiency paradox shows that technical efficiency gains can paradoxically increase aggregate water consumption by enabling crop intensification (Grafton et al., 2018; Ward and Pulido-Velázquez, 2008). Demand-hardening dynamics predict that structural commitment to irrigation infrastructure creates inelastic water demand that amplifies drought vulnerability when supply fails, while annual crop flexibility provides only partial adjustment capacity (Grafton et al., 2018). Whether these mechanisms operate at the watershed scale under a multi-year megadrought remains poorly established. As aridification intensifies across dryland and Mediterranean-climate regions (Gebrechorkos et al., 2025; Zambrano et al., 2025), whether managed irrigation systems buffer or transmit hydroclimatic stress is a critical question for adaptive water governance (FAO y ONU Agua, 2025; Howden et al., 2007; Wallace, 2000). Chile's central Mediterranean zone, where irrigated perennial agriculture draws on Andean snowmelt-fed rivers under a decade-long megadrought (Boisier et al., 2018; Garreaud et al., 2020), provides a natural experiment at the intersection of these questions.

This paper examines how agricultural crop system composition modulates WUE drought sensitivity across 127 Chilean sub-watersheds (2001–2020). Crop composition likely mediates the response to supply constraints: perennial fruit crops maintaining year-round root systems may sustain productivity under partial deficits, whereas annual crops allow area-based adjustment when supply falls critically short (Chakraborti et al., 2023; Davis et al., 2017). The analysis addresses two primary questions: (1) does annual-crop prevalence buffer WUE drought sensitivity independent of the latitudinal aridity gradient, and (2) is irrigation infrastructure

*Corresponding author
Email addresses: fzambrano@udla.cl (Francisco Zambrano), francisco.fernandez@uss.cl (Francisco Fernández), maria.molinos@uva.es (María Molinos-Senante)

prevalence associated with amplified sensitivity consistent with demand-hardening dynamics? Secondary questions address which aridification signal (SPEI, SPI, or EDDI) most strongly predicts WUE variability and whether WUE responses are spatially clustered. Aridification is treated as multi-process using three complementary drought indices: SPEI (Standardized Precipitation Evapostranspiration Index, Vicente-Serrano et al. (2010)) (hydroclimatic balance), SPI (Standardized Precipitation Index, Mckee et al. (1993)) (precipitation deficit), and EDDI (Evaporative Demand Drought Index, Hobbins et al. (2016); McEvoy et al. (2016); AghaKouchak et al. (2015)) (atmospheric evaporative demand). The primary analysis uses a spatial error model framework with 2021 post-drought census crop composition data. All findings are associative; causal inference is not possible given the cross-sectional observational design and spatial confounding.

2. Data and Methods

2.1. Study area

Continental Chile (approximately 17°S to 56°S) spans extreme latitudinal climate gradients, from the hyperarid Atacama in the north to the Mediterranean zone (32°S–38°S) concentrating the majority of irrigated agriculture, viticulture, and fruit export production, and a humid-temperate zone supporting rainfed cereals and forages south of 38°S (Figure 1). The megadrought most severely affected the 30°S–42°S band, where precipitation deficits of 25–45% relative to the twentieth-century mean have persisted since 2010 (Boisier et al., 2018; Garreaud et al., 2020). The study uses watershed-level spatial units based on Chilean National Water Authority (DGA) hydrological boundaries, which align with the country's water allocation governance framework (Rivera et al., 2016). Chile's 1981 Water Code established a privatized, market-based water governance system in which water rights are tradeable property and drought allocation is governed primarily by seniority and market exchange rather than state emergency intervention (Malagueño and D'Odorico, 2024).

2.2. WUE data

Annual cropland WUE ($\mathrm{g\,C\,kg^{-1}\,H_2O\,yr^{-1}}$), defined as $WUE = NPP/ET$, was obtained from the global cropland WUE dataset of Jiang et al. (2025), providing 1-km annual rasters for 2001–2020. NPP was estimated using an Evaporative Fraction Light-Use Efficiency (EF-LUE) model driven by ERA5-Land reanalysis, GLASS fAPAR and LAI, and ESA CCI-LC land cover, calibrated against FLUXNET2015 flux towers across multiple climate zones. ET was obtained from the ETMonitor product (Hu and Jia, 2015), validated against flux towers ($r > 0.75$). WUE rasters were cropped to Chile's extent and annual

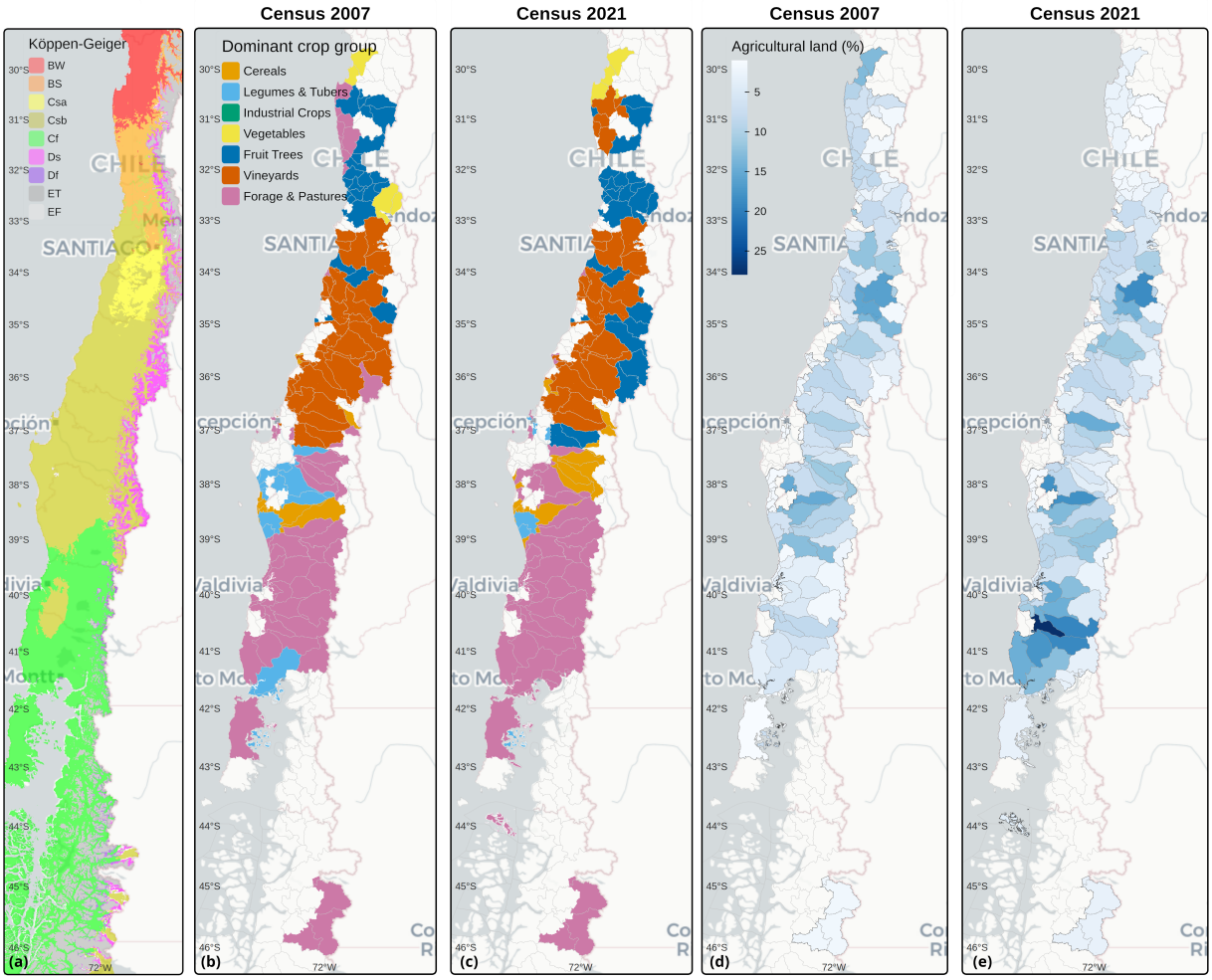

Figure 1: Study area and agricultural context across central Chile. (a) Köppen-Geiger climate classification across the study domain, spanning arid (BW) and semi-arid (BS) zones in the north, the warm- and hot-summer Mediterranean centre (Csa, Csb), and the humid-temperate south (Cf). (b-c) dominant agricultural crop group per sub-watershed, derived from the VII (2007) and VIII (2020-2021) Chilean Agricultural and Forestry Censuses. (d-e) agricultural land as a percentage of total sub-watershed area for the same two census years. Sub-watershed boundaries (DGA) are outlined in grey.

mean WUE was extracted per sub-watershed by spatial averaging. The 20-year series (2001-2020) spans a pre-megadrought reference period (2001-2009) and the megadrought period (2010-2020). The WUE was standardized using z-scores for the years 2001-2020 and will be used in this context.

2.3. Drought drivers and WUE mechanistic components

2.3.1. Aridification drivers

Three complementary drought indices characterize distinct aridification dimensions (AghaKouchak et al., 2015; Zambrano et al., 2025). SPEI (primary driver) captures the hydroclimatic balance incorporating both precipitation and atmospheric evaporative demand (Vicente-Serrano et al., 2010). It was computed from CHIRPS (Climate Hazards Group InfraRed Precipitation with Station data) monthly precipitation (Funk et al., 2015) and FAO-56 Penman-Monteith reference evapotranspiration derived from CHIRTS-daily temperature data (Climate Hazards Center Infrared Temperature with Stations, Funk et al. (2019)), then aggregated to a monthly basis. SPI isolates precipitation deficits from the same CHIRPS series (Mckee et al., 1993). EDDI characterizes anomalies in atmospheric evaporative demand independently of precipitation (Hobbins et al., 2016; McEvoy et al., 2016), computed from CHIRTS-based derived reference evapotranspiration. We used the EDDI sign convention to indicate that positive values represent below-normal evaporative demand, while negative values signify above-normal demand, thereby aligning EDDI with the polarity of SPEI and SPI. Each index was computed at 12, 24, and 36-month accumulation scales. The three indices were standardized via the empirical probability-weighted normal approximation. The December value for each year was retained as the annual index observation.

All three drought indices are derived from CHIRPS precipitation and CHIRTS temperature data, observation-based satellite-gauge merged products independent of the ERA5-Land reanalysis used by the EF-LUE model; the crop composition spatial error model uses relative cross-watershed sensitivity rankings unaffected by any spatially uniform forcing. Mean within-watershed temporal R^2 at the per-family optimal scales was 0.277 for SPEI-12, 0.264 for SPI-12, and 0.168 for EDDI-24; SPEI-12 and SPI-12 show practically equivalent temporal explanatory power (TOST [Two One-Sided Tests] within ± 0.05 margin: $p < 0.001$, 90% CI [+0.007, +0.019]). Drought indices are standardized temporal anomalies relative to each watershed's local historical mean and carry little information about the absolute spatial aridity gradient at any single time point; near-zero unique cross-sectional variance attributable to drought indices is a dimensional artefact of standardization, not evidence that drought matters less than crop composition for WUE. The SPEI–SPI cross-sectional equivalence result is reported in Section 3.4.

2.3.2. *WUE mechanistic components*

We used the NPP (MOD17A3HGF, MODIS Terra, 500 m, Collection 6.1), which was z-score standardized within 2001-2020 (zNPP), which will be called NPP hereafter; and SETI-12 (Paruelo et al., 2016) (Standardized Evapotranspiration Index, 12-month scale; derived from MOD16A2GF actual evapotranspiration Running et al. (2021)). These are used exclusively as descriptive spatial context variables for the trend comparison in Section 3.1. The primary CASEarth WUE dataset does not distribute its internal NPP (EF-LUE model) and ET (ETMonitor) component layers separately, making algebraic decomposition infeasible. Because MOD17 and MOD16 have different sensitivities and error structures from the EF-LUE and ETMonitor models, NPP and SETI-12 are not used for formal component attribution of WUE variance, and no cross-product comparison of their relative sensitivities is presented.

2.4. *Agricultural census data*

Crop composition data were obtained from the VII Census (2007, pre-drought baseline) (INE, 2007) and the VIII Census (2020–2021, endpoint) (INE, 2021), both reporting cultivated area by crop category and management type at commune level. Commune-level data were spatially aggregated to sub-watershed level using area-weighted means. Three functional aggregates were computed for use as regression predictors: *pct_perennials* (fruit trees + vineyards), *pct_annuals* (cereals + vegetables + legumes + industrial crops), and *pct_forage* (forage/pasture; reference category). The variable *pct_irrigated* measures the census-reported proportion of agricultural land classified as irrigated, reflecting irrigation infrastructure and historical water rights, not the volume of water actually delivered in any given year. Sub-watersheds with high *pct_irrigated* have more irrigation-dependent cropping systems and greater structural exposure to supply disruptions. Dominant crop type per watershed was assigned using a 40% area threshold.

The 2021 census irrigated area variable is derived entirely from directly reported data and underpins the primary spatial error model results. The 2007 irrigated area variable required partial imputation for six of ten crop categories using a commune-level residual ratio; because this single ratio is applied uniformly across categories with very different true irrigation intensities, it fundamentally distorts the cross-sectional variance structure of the 2007 pct_irrigated variable, and measurement error in this predictor spills over to bias the coefficients of correlated predictors in the same multiple regression. The 2007 model is therefore reported only in Supplementary Table S-9 and cannot support temporal comparisons for any predictor. Full imputation details and code are available at the project repository.

2.5. Statistical analyses

2.5.1. Trend and change-point analyses

Mann-Kendall trend tests and Sen's slope estimates (with prewhitening) were computed per watershed for WUE, NPP, SETI-12, and EDDI-12 (2001-2020). The Pettitt test (Pettitt, 1979) was applied to each WUE series to detect the most probable year of mean-level shift. Benjamini-Hochberg (BH) false-discovery-rate (FDR) correction was applied across 131 simultaneous tests. Watersheds were classified by significance ($p < 0.05$) and proximity to megadrought onset (break years within ± 2 years of 2010). A permutation null model (B = 1000 iterations per watershed, seed = 2026) tested whether the observed break-year concentration near 2010 is distinguishable from a SPEI-step-change tracking null. Within-watershed residuals from a SPEI-12 OLS (ordinary least squares) regression were resampled with replacement and the Pettitt test was re-run on each reconstructed null series. Observed and null break-year distributions were compared using a two-sample Kolmogorov-Smirnov (KS) test. Mean WUE was compared between the pre-megadrought (2001-2009) and megadrought (2010-2020) periods using Wilcoxon signed-rank tests, stratified by Köppen climate class.

2.5.2. WUE-aridification relationships

Spearman correlations and OLS sensitivity slopes ($\Delta WUE/\Delta Index$) were computed per watershed across the 20-year series. Per-watershed maps are treated as descriptive summaries given strong spatial autocorrelation (Moran's I = 0.509-0.683); confirmatory inference rests on the spatial error models and FDR-corrected Pettitt analysis. Moran's I and Getis-Ord Gi* local statistics identified spatial clustering and hotspots of WUE trend slope using queen contiguity weights. A two-way fixed-effects (TWFE) panel regression estimated:

$$WUE_{it} = \beta \cdot Index_{it} + \mu_i + \tau_t + \varepsilon_{it} \tag{1}$$

where μ_i and τ_t are watershed and year fixed effects. Standard errors are Driscoll-Kraay (DK; Driscoll and Kraay (1998); bandwidth = 2), consistent for both serial correlation and cross-sectional spatial dependence. DK SEs (standard errors) inflate 3-4× relative to conventional HC1 (Heteroskedasticity-Consistent) clustered SEs, reflecting the strong spatial common component (full comparison in Supplementary Table S-11).

2.5.3. Crop composition and WUE sensitivity

The per-watershed OLS slope of WUE regressed on SPEI-12 was used as the outcome in a multiple regression:

$$Sensitivity_i = \beta_0 + \beta_1 \cdot pct\_perennials_i + \beta_2 \cdot pct\_annuals_i + \beta_3 \cdot pct\_irrigated_i + \varepsilon_i \quad (2)$$

with forage/pasture as the reference category. Variance inflation factors confirmed the absence of harmful multicollinearity (all VIF < 5). Where OLS residuals were spatially autocorrelated (Moran's I, $p < 0.05$), a spatial error model (SEM) was fitted as the primary inferential model.

The TWFE panel introduced in Section 2.5.2 is estimated over the same 127 sub-watersheds; its non-significant Driscoll-Kraay results (Section 3.5) may appear to undermine the two-stage SEM, but the two approaches ask fundamentally different questions and address distinct statistical quantities. The panel estimates the *pooled mean* $\bar{\beta} = E[\beta_i]$, Driscoll-Kraay SEs make this uncertain because contemporaneous cross-sectional dependence reduces the effective independent information available to pin down the common temporal slope. The SEM, by contrast, uses the *cross-sectional dispersion* of per-watershed slopes β_i, testing whether irrigation-dense watersheds show systematically larger β_i than rainfed watersheds. These are separable quantities, $E[\beta_i]$ can be uncertain while $\mathrm{Var}(\beta_i)$ is real and structured. A concern that per-watershed OLS slopes are "spurious" because they capture a common year-effect conflates these two estimands. When a common drought signal simultaneously depresses SPEI across all watersheds, β_i measures how strongly each watershed's WUE co-moves with that signal, a valid and interpretable measure of local coupling strength. An irrigation-dense watershed with $\beta_i = 0.8$ genuinely shows stronger drought coupling than a rainfed watershed with $\beta_i = 0.1$, regardless of whether the pooled mean is identifiable. Moran's I $= 0.514$ ($p < 0.001$) on the observed β_i values confirms this cross-sectional variation is spatially organized rather than noise.

A supplementary pre-drought comparison using the 2007 census is reported in Supplementary Table S-9; as detailed in Section 2.4, imputation issues render it uninformative for all three predictors. Robustness was verified through: (i) restriction to within-Csb warm-summer Mediterranean sub-watersheds (n = 67); (ii) a synchronized-time bootstrap (B = 1000) propagating stage-1 estimation uncertainty while preserving cross-sectional spatial covariance (Supplementary Table S-10); (iii) a barren-exclusion dynamic land-cover filter excluding MODIS-confirmed non-vegetated pixels (Supplementary Table S-7); (iv) a parallel SEM using the Standardized Snow Water Equivalent Index (SWEI) from ERA5-Land as the drought predictor (Supplementary Table S-6); and (v) addition of sub-watershed centroid latitude as a direct covariate to test whether the irrigation association persists after explicit control for the latitudinal aridity gradient (Table 1).

2.6. Software

All statistical analyses and spatial processing were conducted in R (v4.5.2; R Core Team (2025)). Raster operations and spatial aggregation used `terra` (v1.8.54; Hijmans (2025)). Vector geometries and spatial joins used `sf` (v1.0.23; Pebesma (2018), Pebesma and Bivand (2023)). Spatiotemporal array operations used `stars` (v0.6.8; Pebesma and Bivand (2023)). Mann-Kendall trend tests and Sen's slope estimation with prewhitening used `modifiedmk` (v1.6; Patakamuri and O'Brien (2021)) and `trend` (v1.1.6; Pohlert (2023)). Spatial autocorrelation (Moran's I, Getis-Ord Gi*) and spatial weight matrices used `spdep` (v1.4.1; Bivand and Wong (2018)). Spatial Error Model was made using `{spatialreg}` (Bivand et al., 2021). Panel regression with fixed effects used `plm` (Croissant and Millo, 2008); Driscoll-Kraay standard errors via `plm::vcovSCC` (Driscoll and Kraay, 1998); HC1 clustered SEs via `plm::vcovHC` with `lmtest::coeftest`. Variance inflation factors used `car` (v3.1.3; Fox and Weisberg (2019)). General-purpose data manipulation and reshaping used `tidyverse` (v2.0.0; Wickham et al. (2019)), including `dplyr`, `tidyr`, `readr`, `stringr`, `purrr`, and `lubridate`. Thematic maps used `tmap` (v4.2; Tennekes (2018)). Statistical graphics used `ggplot2` (v3.5.2; Wickham (2016)). Multi-panel figure layout used `patchwork` (v1.3.1; Pedersen (2025)).

3. Results

3.1. Long-term WUE trends

Trend analysis across 127 Chilean agricultural sub-watersheds revealed predominantly negative WUE trends across the Mediterranean-climate zone (approximately 30°S–35°S), consistent with megadrought onset and intensification (Figure 2).

NPP (MOD17A3HGF) and SETI-12 (MOD16A2GF) are independent proxy products that do not decompose the CASEarth WUE directly; the following patterns are descriptive spatial co-variation, not formal component attribution. NPP trends exhibit strong spatial covariance with WUE, with negative anomalies concentrated in the same central Mediterranean watersheds where WUE declines are most pronounced. SETI-12 trends are more spatially complex: sub-watersheds where ET declined less steeply than NPP tend to show WUE decline, while those where ET reduction exceeded NPP reduction tend toward stable or improving WUE. Declining WUE is spatially co-located with negative NPP anomalies, while ET responses are heterogeneous and modulated by irrigation access and crop type. Whether NPP suppression is a more proximate correlate of WUE decline than ET cannot be formally established from these proxy data, as the independent products may differ in sensitivity and error structure from the EF-LUE and ETMonitor components underlying the CASEarth WUE (Fifth limitation, Section 4.5).

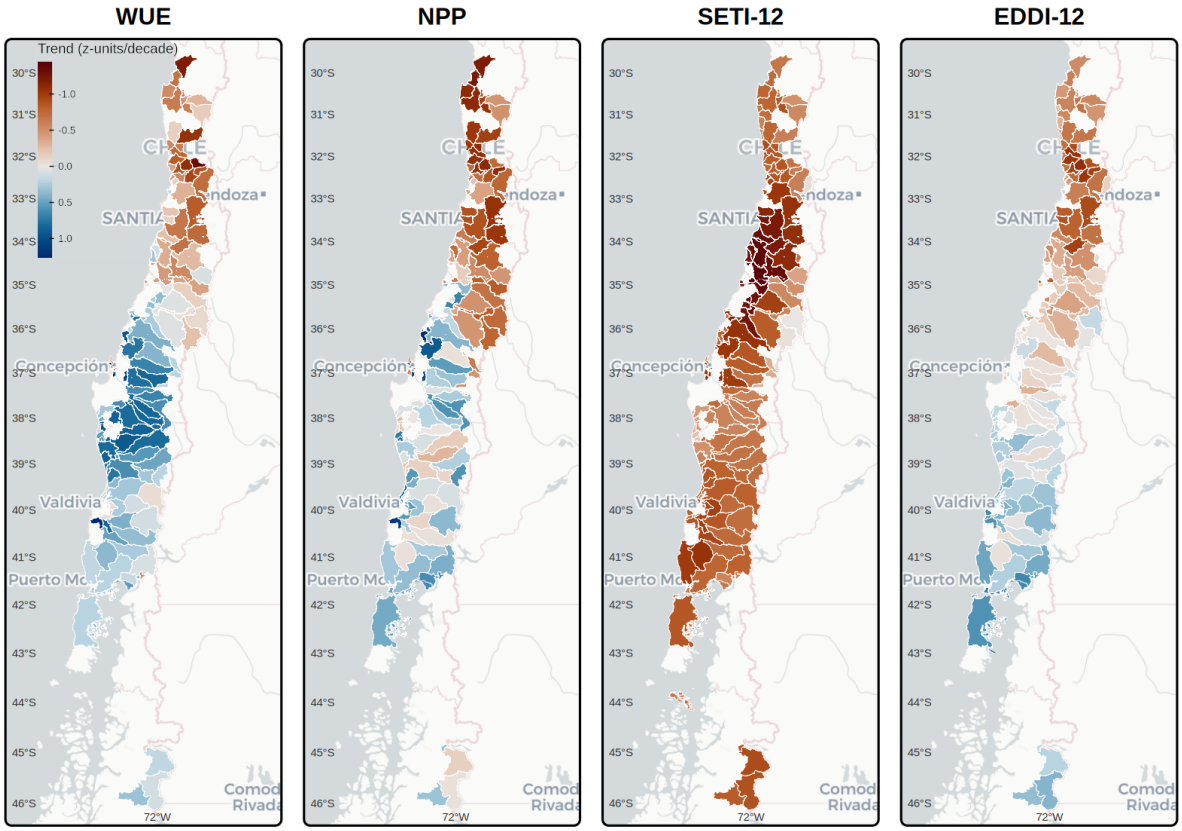

Figure 2: Spatial distribution of long-term trends in zWUE (WUE anomaly), zNPP (NPP anomaly), SETI-12 (12-month ET anomaly), and EDDI-12 (12-month atmospheric evaporative demand) across Chilean watersheds (2001-2020). Trend magnitudes are expressed as z-score standardized Sen's slope estimates.

3.2. WUE change-point analysis

The Pettitt test detected FDR-significant mean-level change points in 22 of 131 sub-watersheds (adjusted p range: 0.019–0.047), all dated 2009–2012. The permutation null model showed that 72.1% of null Pettitt tests also had break years within ±2 years of 2010 (observed: 84.1%); the Kolmogorov-Smirnov test detected no significant difference ($D = 0.153$, $p = 0.255$), a failure to reject the null. The observed break-year concentration near 2010 is therefore not distinguishable from what would be expected under SPEI-step-change tracking alone. Break years were not significantly spatially clustered (Moran's $I = 0.018$, $p = 0.345$), consistent with common large-scale forcing rather than spatial propagation. The geographic distribution of FDR-significant breaks, concentrated in the central Mediterranean zone while the arid north and wet south show no aligned breaks (Boisier et al., 2018; Garreaud et al., 2020), is provided for descriptive reference (Figure 3 a).

3.3. WUE before and after the megadrought

Mapping $\Delta WUE = WUE_{post} - WUE_{pre}$ per watershed revealed pronounced spatial heterogeneity (Figure 3 b). Arid and semi-arid sub-watersheds showed predominantly negative ΔWUE, while irrigated Mediterranean and humid-temperate sub-watersheds showed positive ΔWUE. The aggregate Wilcoxon signed-rank test was positive and significant ($p = 0.007$), but this reflects the numeric dominance of irrigated Mediterranean sub-watersheds, not widespread drought resilience. Köppen-stratified analyses resolve the heterogeneity (Supplementary Table S-2). BW (hot desert; $n = 8$) showed significant declines (Hodges-Lehmann [HL] estimate = −0.535, 95% Confidence Intervals [CI]: −0.862 to −0.335; $p = 0.008$), as did BS (semi-arid steppe; $n = 14$; HL = −0.643, $p < 0.001$). Csb (warm-summer Mediterranean; $n = 71$) and Cf (humid subtropical; $n = 26$) exhibited significant WUE increases (HL = +0.374, $p < 0.001$ and HL = +0.367, $p < 0.001$, respectively). Violin-boxplot distributions stratified by Köppen class (Figure 3 c) confirm this divergence.

3.4. WUE responses to aridification signals

Spearman correlation analysis at the per-family optimal scales (SPEI-12, SPI-12, EDDI-24) revealed positive associations between annual WUE and drought indices across most Chilean watersheds (Figure 4), with wetter years generally associated with higher WUE.

At the 36-month scale, SPEI and SPI showed practically equivalent associations with WUE (mean R^2 = 0.240 and 0.229; TOST within ±0.05 margin: $p < 0.001$, 90% CI [−0.004, +0.003]), both significantly outperforming EDDI-36 (mean $R^2 = 0.140$; $p < 0.001$; Supplementary Figure S-2). The precipitation component dominates the spatial gradient in WUE variability at multi-year accumulation scales.

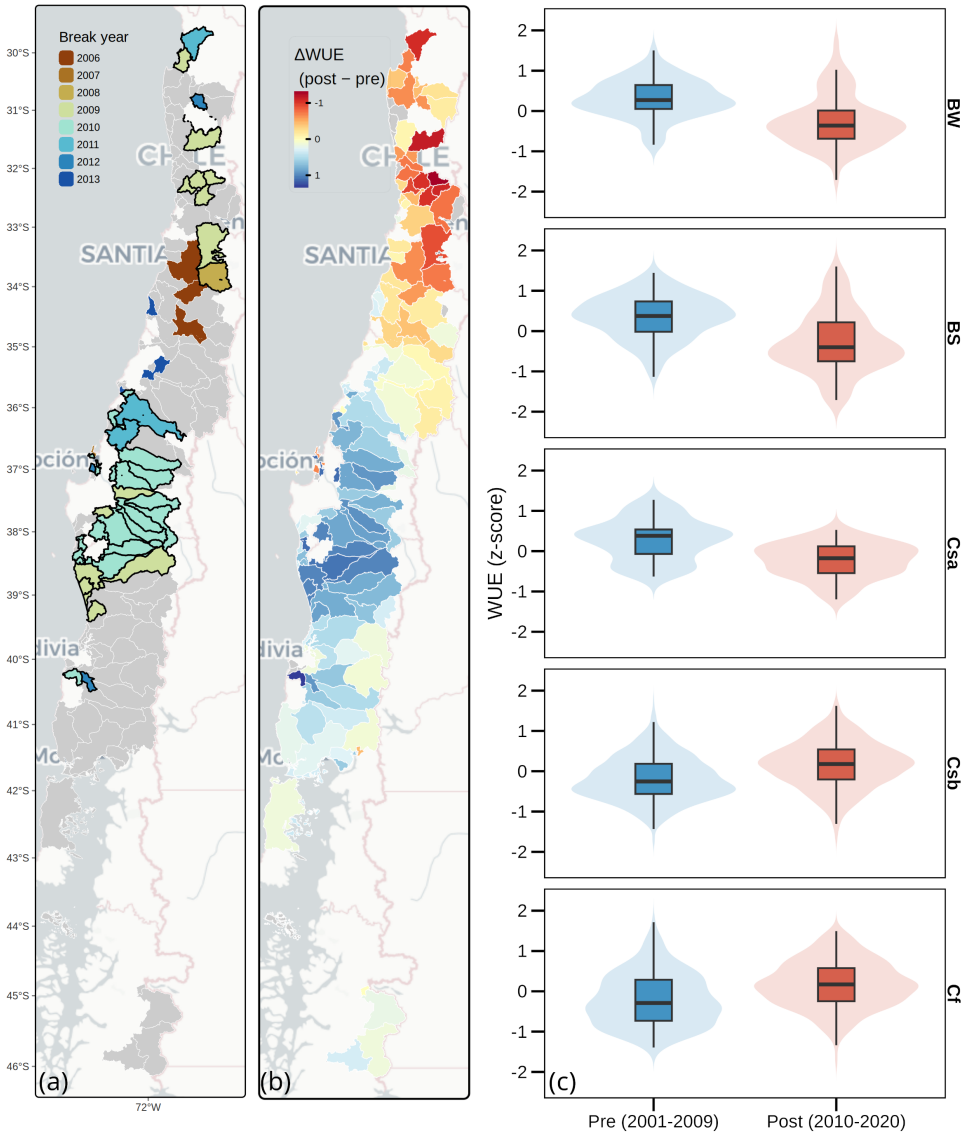

Figure 3: (a) Spatial distribution of Pettitt change-point years in annual WUE per watershed (FDR-significant at adjusted $p < 0.05$). Watersheds with change-point years within ±2 years of 2010 are highlighted with bold borders. FDR-significant breaks concentrate in the central Mediterranean zone; the permutation null model does not distinguish this concentration from SPEI-step-change tracking (KS $p = 0.255$; Section 3.2). Provided for descriptive geographic reference. Non-significant change points are shown in grey. (b) Spatial map of WUE change between the megadrought period (2010–2020) and the pre-megadrought period (2001–2009) ($\Delta WUE = WUE_{post} - WUE_{pre}$) per watershed. Positive values (blue) indicate net WUE increase; negative values (red) indicate WUE decline. Köppen climate zone boundaries (dashed lines) are overlaid. (c) Violin-boxplot distributions of annual WUE for the pre-megadrought (blue, 2001–2009) and megadrought (red, 2010–2020) periods, stratified by Köppen climate class. Each panel corresponds to one climate class; y-axes are free-scaled.

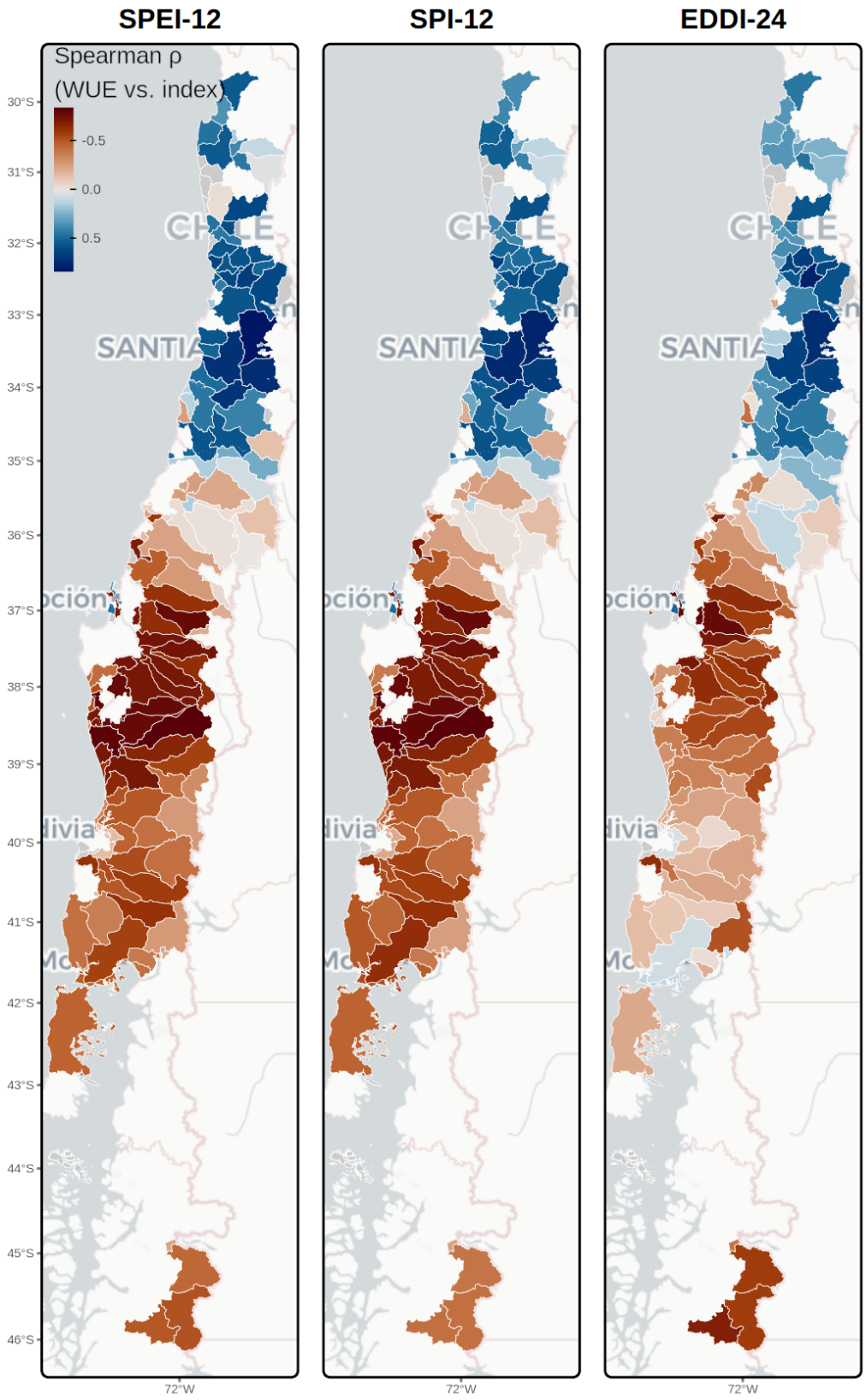

Figure 4: Spatial maps of Spearman (WUE vs. drought index) per watershed, faceted by drought index at the accumulation scales used for the per-watershed spatial analyses (SPEI-12, SPI-12, EDDI-24). Diverging colour scale (blue = positive correlation, red = negative correlation).

3.5. Panel regression: temporal WUE-drought relationships

Under Driscoll-Kraay standard errors, no panel coefficient reaches conventional significance at any index or accumulation scale. SPEI-12 ($\beta = -0.112$, DK $p = 0.273$), SPI-12 ($\beta = -0.170$, DK $p = 0.053$), and Mediterranean-restricted SPEI-24 ($\beta = +0.193$, DK $p = 0.458$) and SPI-24 ($\beta = +0.141$, DK $p = 0.579$) are all non-significant (Supplementary Table S-11). The negative signs at the 12-month scale arise from humid-temperate Cf sub-watersheds (n = 26), where rainfed annual systems transiently raise WUE under mild moisture stress (Yu et al., 2020). The substantive interpretation is that WUE-drought co-variation in the temporal panel is largely a spatially common signal. The same calendar years are simultaneously wet or dry across all Mediterranean watersheds, leaving insufficient independent within-unit variation to support inference once cross-sectional dependence is properly accounted for. The drought index's physical role in determining WUE sensitivity is established through the cross-sectional sensitivity slopes (Section 3.6, Section 3.7) and the DGA streamflow validation (Section 4.3), not through the panel temporal analysis. Full HC1 vs. DK comparison is in Supplementary Table S-11. A linear HC1 post-2010 interaction model at SPEI-36 yields a positive intensification term ($\beta = +0.281$, $p = 0.012$; Supplementary Figure S-6), but Supplementary Table S-8 shows this pattern is attributable to the concentration of strongly negative SPEI-36 values after 2010 operating on a concave WUE-SPEI relationship, not a discrete temporal structural break.

3.6. Spatial distribution and clustering of WUE sensitivity

The WUE-SPEI-12 sensitivity map (Figure 5 a) shows the OLS slope per watershed. Sensitivity broadly follows the latitudinal aridity gradient, with central Mediterranean watersheds exhibiting higher values than humid southern watersheds and locally elevated sensitivity in perennial-dominated irrigated zones (Figure 5 b and c).

Moran's I for WUE trend slope was I = 0.683 ($p < 0.001$) and for WUE-SPEI-12 R^2 was I = 0.509 ($p < 0.001$), confirming strong geographic clustering. Getis-Ord Gi* hotspot analysis identified coherent coldspots in the central Mediterranean zone and localized hotspots in transitional zones (Figure 5 d). Pettitt change-point years were not significantly spatially clustered (I = 0.018, p = 0.345), indicating that the temporal concentration near 2010 reflects common large-scale forcing rather than spatial propagation. Hydroclimate governs when and how strongly WUE shifts over time; crop composition modulates the spatial magnitude of each sub-watershed's drought sensitivity. These two axes are complementary rather than competing.

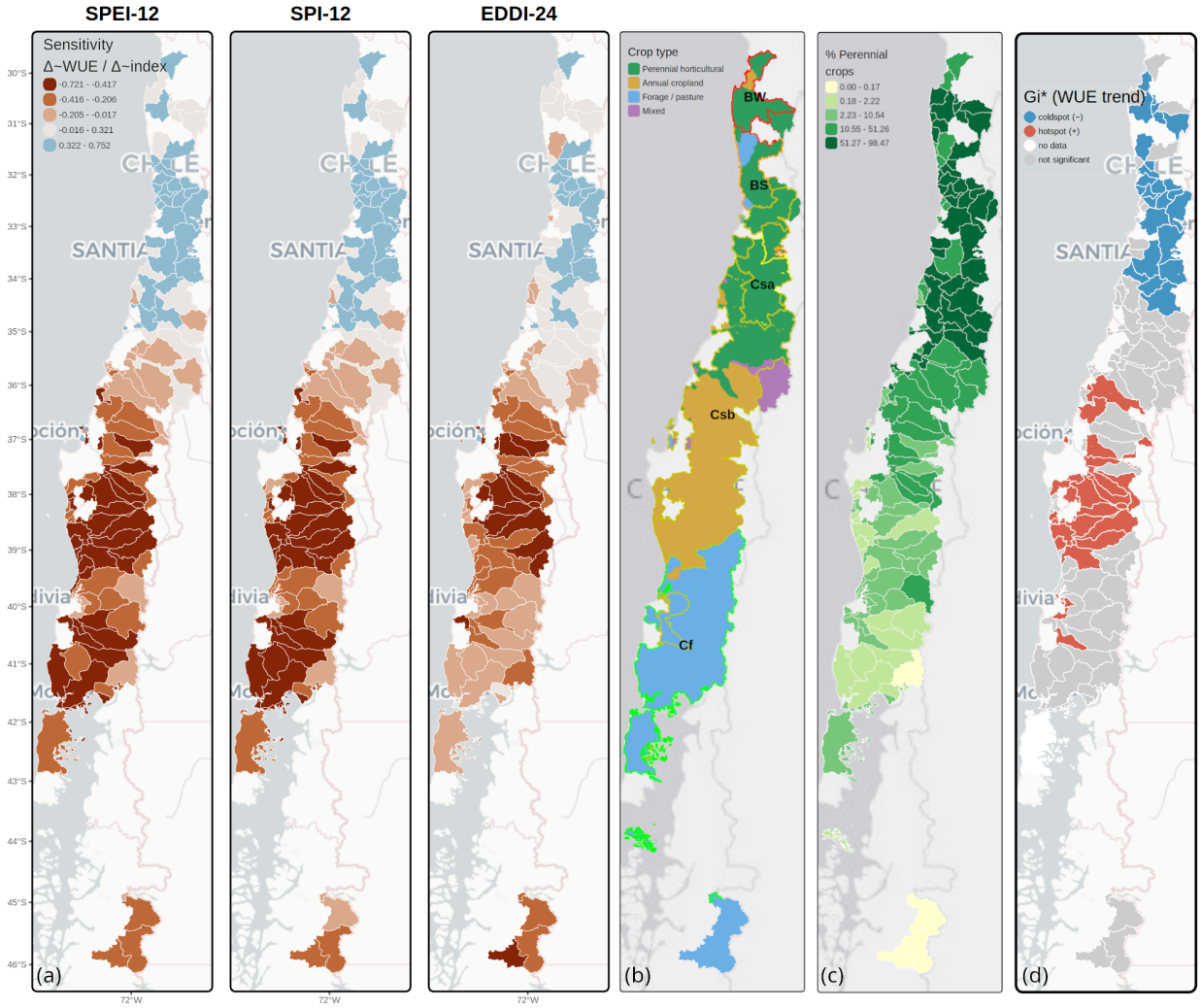

Figure 5: (a) Spatial distribution of WUE-drought sensitivity ($\Delta WUE/\Delta Index$, the OLS slope of the annual WUE ~ index regression per watershed, 2001-2020) for SPEI-12, SPI-12, and EDDI-24. High positive values indicate strong positive WUE response; near-zero or negative values indicate weak or inverted coupling. (b) Choropleth map of dominant crop type per watershed, classified by the agricultural functional group exceeding 40% of total agricultural area (Perennial horticultural, Annual cropland, Forage/pasture, Mixed). (c) Choropleth map of perennial crop share (% of total agricultural area under fruit trees and vineyards) per watershed. (d) Getis-Ord Gi* hotspot analysis of WUE trend slope across Chilean watersheds. Red watersheds are statistically significant hotspots (positive WUE trend clusters; Gi* > 1.96); blue are coldspots (negative WUE trend clusters; Gi* < -1.96); grey are not significant at the 95% level.

3.7. Agricultural crop composition and WUE sensitivity

Integration of census-derived crop composition with WUE-SPEI-12 sensitivity estimates (n = 127 sub-watersheds) revealed contrasting patterns by crop system. Annual cropland sub-watersheds showed lower sensitivity than forage/pasture watersheds, while perennial horticultural sub-watersheds showed the highest median sensitivity (Figure 6 a); because perennial crop distribution, aridity, and WUE sensitivity all co-vary with latitude (Figure 7 c), the perennial pattern likely reflects the underlying climate gradient rather than an isolated crop-system effect (Section 4.5). Irrigated area share was positively associated with sensitivity in the full-sample pooled analysis (Figure 7 a).

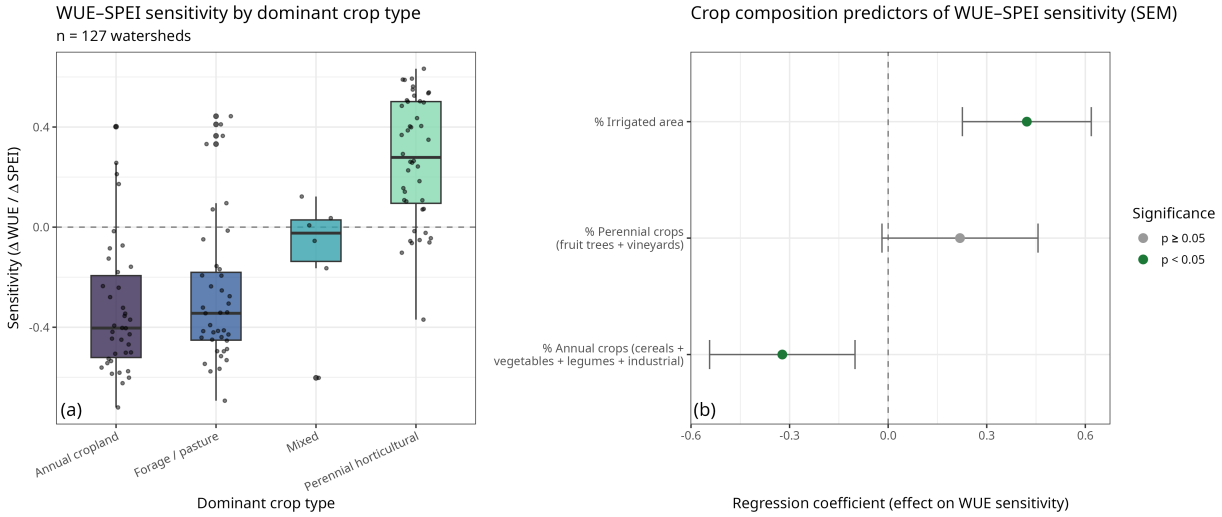

Figure 6: WUE-SPEI-12 sensitivity by dominant crop type (n = 127 sub-watersheds). (a) Boxplot distributions of per-watershed OLS sensitivity slopes stratified by dominant agricultural system: perennial horticultural (fruit trees + vineyards), annual cropland (cereals + vegetables + legumes + industrial crops), mixed systems (no single group exceeds 40% of agricultural area), and forage/pasture. Perennial-dominated watersheds show the highest median sensitivity; forage/pasture watersheds show the lowest. (b) Full-sample SEM coefficient plot for the three functional-aggregate predictors (perennial crops, annual crops, irrigated area; reference: forage/pasture) with 95% confidence intervals; filled symbols indicate p < 0.05. Numeric values and within-Csb comparisons are in Table 1.

The multivariate OLS regression (n = 127 sub-watersheds) returned: annual crop share as a significant negative predictor ($\beta = -0.304$, $p < 0.001$), indicating buffering relative to the forage/pasture reference; perennial crop share as a positive but subsequently attenuated predictor ($\beta = 0.359$, $p = 0.003$); and irrigated area share as the strongest positive predictor ($\beta = 0.499$, $p < 0.001$), reflecting the association between irrigation infrastructure prevalence and drought coupling rather than actual water volumes delivered in drought years.

Moran's I on OLS residuals was I = 0.197 ($p = 0.001$), so a spatial error model (SEM; queen-contiguity weights) was fitted as the primary inferential model ($\lambda = 0.468$, $p < 0.001$). The SEM attenuated but largely

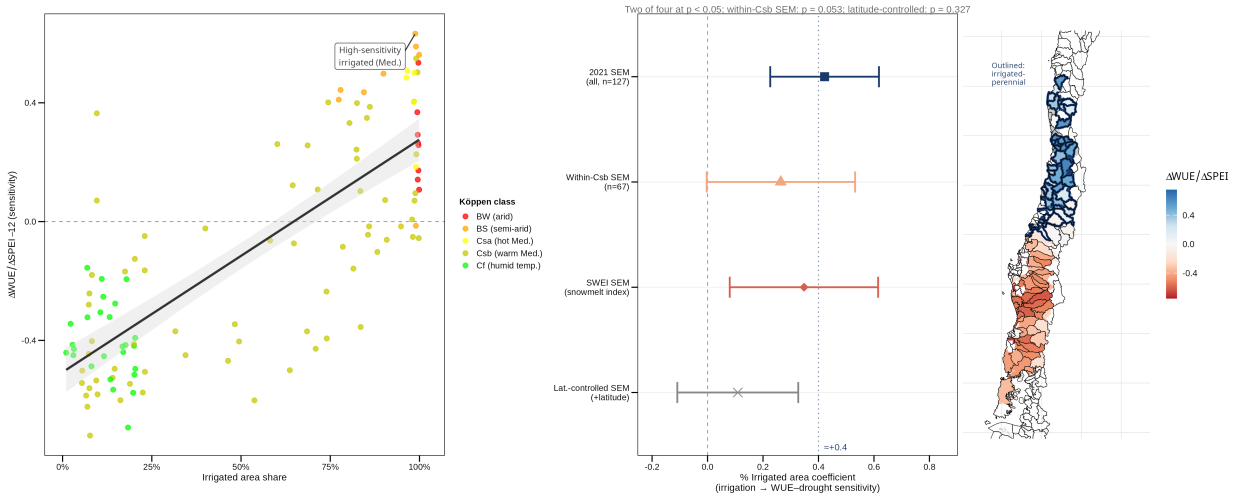

Figure 7: (a) Scatter plot of WUE-SPEI-12 sensitivity versus irrigated area share per sub-watershed (n = 127), coloured by Köppen climate class, with a pooled OLS regression line (±95% CI). Points in the upper-right cluster (high irrigation, high sensitivity) correspond to Mediterranean irrigated-perennial systems; points in the lower-left correspond to rainfed or annual-crop dominated systems. (b) Forest plot of the irrigated area share regression coefficient (±95% CI) across four model specifications: 2021 full-sample SEM, within-Csb warm-summer Mediterranean SEM, SWEI-based SEM using snowmelt index as the drought predictor, and a latitude-controlled SEM with watershed centroid latitude added as a covariate. The 2007 pre-drought SEM is omitted from this figure because imputation issues render it uninformative (Supplementary Table S-9). Two specifications are significant at $p < 0.05$ (full-sample SEM and SWEI SEM); the within-Csb SEM is marginal (= +0.264, p = 0.053); the latitude-controlled SEM attenuates to = +0.109 (p = 0.327), consistent with partial confounding by the latitudinal aridity gradient. The vertical dotted line marks +0.4 for reference. (c) Choropleth of WUE-SPEI-12 sensitivity (OLS slope per watershed, 2001–2020); solid blue borders outline perennial-horticultural-dominant sub-watersheds, which concentrate in the central Mediterranean zone and correspond to the high-sensitivity cluster in panel (a).

preserved the OLS conclusions: annual crop share ($\beta = -0.322$, $p = 0.004$), perennial crop share ($\beta = 0.219$, nominal $p = 0.071$; Figure 6 b), and irrigated area share ($\beta = 0.422$, $p < 0.001$). A synchronized-time bootstrap (Supplementary Table S-10) confirmed significance for all three predictors ($p = 0.002$-0.032) with bootstrap SEs 0.74-0.91× nominal; WLS estimates (Supplementary Table S-5) confirm no sign changes under stage-1 uncertainty weighting.

To test whether associations are crop-system properties robust to the latitudinal aridity gradient, the model was restricted to Csb warm-summer Mediterranean sub-watersheds (n = 67). Results differ strikingly by predictor (Table 1):

Table 1. Comparison of WUE-SPEI-12 sensitivity regressions across model specifications. Full-sample SEM: n = 127 (all climate classes); within-Csb OLS and SEM: n = 67 (warm-summer Mediterranean, $\lambda = 0.255$, $p = 0.057$); latitude-controlled SEM: n = 127 with sub-watershed centroid latitude added as a covariate. Reference category: forage/pasture. *** $p < 0.001$; ** $p < 0.01$; * $p < 0.05$; † $p < 0.10$. Full model outputs in Supplementary Tables S-4 (within-Csb) and S-14 (latitude-controlled).

Predictor	Full-sample SEM	Full-sample SEM p	Within-Csb OLS β	Within-Csb OLS p	Within-Csb SEM β	Within-Csb SEM p	Lat.-controlled SEM β	Lat.-controlled SEM p
% Irrigated area	+0.422	< 0.001 ***	+0.317	0.016 *	+0.264	0.053 †	+0.109	0.327
% Annual crops	−0.322	0.004 **	−0.463	0.004 **	−0.565	0.001 **	−0.485	< 0.001 ***
% Perennial crops	+0.219	0.071 †	+0.297	0.102	+0.184	0.320	+0.025	0.833

The annual-crops association strengthens within Csb (SEM $\beta = -0.565$, $p = 0.001$), confirming it as a genuine crop-system property independent of the latitudinal gradient. Perennial crop share is non-significant in all specifications (full-sample SEM $p = 0.071$; within-Csb SEM $p = 0.320$), consistent with its inseparability from the latitudinal aridity gradient. The irrigated area association survives the Csb restriction in OLS ($\beta =$

+0.317, $p = 0.016$), attenuating to marginal significance under SEM within Csb ($\beta = +0.264$, $p = 0.053$; Figure 7 b).

A direct latitude-control test, adding sub-watershed centroid latitude as a covariate to the full-sample SEM, is presented in Table 1 (rightmost columns). The irrigation coefficient attenuates from $\beta = +0.422$ to $\beta = +0.109$ ($p = 0.327$; ΔAIC = 20.4), confirming partial confounding with the latitudinal aridity gradient. The annual-crops coefficient strengthens ($\beta = -0.485$, $p < 0.001$), establishing annual-crop buffering as the more latitude-robust result. The perennial coefficient collapses to near zero ($\beta = +0.025$, $p = 0.833$).

The pre-drought census comparison is reported in Supplementary Table S-9; imputation issues render it uninformative for distinguishing structural from adaptive effects (Section 2.4). The causal direction of the 2021 negative association is discussed in Section 4.3.

Natural vegetation contamination within the agricultural mask was non-significant as a control covariate ($\beta = 0.098$, $p = 0.509$; Supplementary Figure S-3).

4. Discussion

4.1. The megadrought as a driver of persistent WUE change

That WUE undergoes a mean-level shift concurrent with the megadrought onset is a physically expected consequence of WUE being hydroclimate-driven, not a novel finding. The permutation null model provides no evidence to distinguish the observed break-year concentration from simple SPEI step-change tracking (KS p = 0.255), confirming this expectation. The geographic distribution of FDR-significant breaks, concentrated in the central Mediterranean zone, is descriptively consistent with megadrought forcing but does not establish coupling beyond what SPEI-step-change tracking alone would produce. The aggregate WUE increase (Wilcoxon p = 0.007) masks pronounced spatial heterogeneity: arid northern sub-watersheds declined while the irrigated Mediterranean zone rose, coinciding with the elevated drought coupling documented in Section 4.3.

4.2. Multidimensional aridification: why index choice matters

The practically equivalent performance of SPEI-36 and SPI-36 in cross-sectional analyses (TOST: p < 0.001) indicates that the precipitation component dominates the spatial gradient in WUE sensitivity under megadrought conditions. The TWFE panel provides no statistically significant evidence for within-unit temporal WUE-drought coupling at any index or scale once cross-sectional dependence is accounted for

through Driscoll-Kraay SEs (Supplementary Table S-11). The substantive interpretation is that WUE-drought co-variation in the temporal panel is largely a spatially common phenomenon. The same calendar years are wet or dry across all Mediterranean watersheds simultaneously, leaving insufficient independent within-unit variation to support inference. Drought's physical role in determining WUE sensitivity is established through the cross-sectional sensitivity slopes and the DGA streamflow validation, not through the panel temporal analysis.

4.3. Irrigation infrastructure and WUE drought sensitivity

In the full-sample SEM, irrigated area share is positively associated with WUE-drought sensitivity ($\beta = +0.422$, $p < 0.001$), with snowmelt co-variation supported by ρ(SPEI-12, DGA streamflow) = 0.72-0.83 and ρ(streamflow, WUE) = 0.38-0.68 in the three northern basins (Supplementary Table S-13). Adding centroid latitude attenuates this to non-significance ($\beta = +0.109$, $p = 0.327$; Table 1), while the within-Csb restriction retains a marginal association ($\beta = +0.264$, $p = 0.053$). The evidence does not contradict demand-hardening dynamics (Grafton et al., 2018; Ward and Pulido-Velázquez, 2008) but cannot establish the irrigation association as latitude-independent.

The annual-crops association is robust to latitude control, strengthening from $\beta = -0.322$ to $\beta = -0.485$ when latitude is added (Table 1); the causal direction is ambiguous and is addressed in limitation (vii).

The perennial crop coefficient is non-significant in all specifications (full-sample p = 0.071; within-Csb SEM p = 0.320; latitude-controlled p = 0.833; Table 1), most plausibly reflecting statistical inseparability from the irrigation coefficient in Chile's Mediterranean zone, where irrigation enables perennial cultivation that creates inelastic water demand (Grafton et al., 2018). Both associations are hypotheses consistent with the data, each constrained by a distinct confound, and should not be interpreted as established causal mechanisms (Boser et al., 2024; FAO y ONU Agua, 2025; Hellegers and Van Halsema, 2021; Wang et al., 2024).

4.4. Spatial structure, global implications, and limits of adaptation

WUE coldspots are concentrated in the Aconcagua, Maipo, Rapel, Mataquito, and Maule basins (32-36°S), precisely the zone concentrating Chile's export fruit and wine production. Because the central agricultural corridor stresses simultaneously, water-market transfers under Chile's privatized Water Code have limited scope to buffer basin-scale shortfalls (Budds, 2020; Malagueño and D'Odorico, 2024; Rivera et al., 2016). Drought-driven WUE decline means more water is consumed per unit of biomass produced; sustaining

production in high-sensitivity basins requires proportionally greater withdrawals precisely when supply is lowest.

The supply-failure mechanism applies conceptually to snowmelt-dependent irrigated agriculture globally (Barnett et al., 2008; Immerzeel et al., 2020; Lutz et al., 2014), but the quantitative crop composition model is a within-Chile spatial descriptor and does not transfer geographically (Figure 8); the mechanism is portable, the coefficients are not. Institutional buffering capacity also differs substantially: Chile's privatized water market, where simultaneous basin-scale droughts exhaust reallocation capacity, represents one end of a governance spectrum, while state-managed systems with groundwater banking may partially decouple farm-gate delivery from meteorological signals.

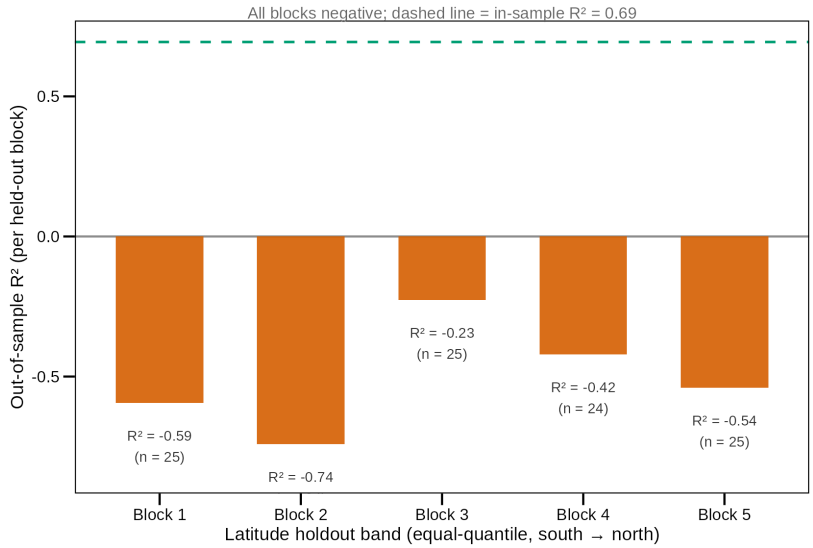

Figure 8: Geographic cross-validation of the crop composition-WUE-SPEI-12 sensitivity model. Continental Chile was partitioned into five equal-latitude-quantile holdout bands (ordered south to north); each band was predicted from a model trained on the remaining four. All five per-block out-of-sample R^2 values are negative (range -1.56 to -0.30), well below the in-sample R^2 of 0.69 (dashed line), meaning the model predicts a held-out latitude band worse than that band's own mean. The quantitative coefficients are not geographically portable; only the supply-failure mechanism transfers conceptually to other snowmelt-dependent irrigation systems.

Where irrigation supply is hydrologically coupled to the same climate signals that drive drought, expanding irrigation infrastructure without securing supply independence may increase aggregate drought exposure. This does not argue against irrigation per se, but distinguishes between systems with independent supply and those coupled to snowmelt and precipitation, a distinction with direct relevance for investment prioritization and drought-contingency planning (FAO y ONU Agua, 2025).

The coldspot concentration in the five key basins is quantifiable in terms directly relevant to water allocation and planting decisions. Sub-watersheds in the Aconcagua and Maipo basins show the highest mean WUE-

SPEI-12 sensitivities in the dataset (mean $\beta = 0.45$ and 0.54 respectively; individual sub-watershed peaks of 0.50 and 0.63), combined with near-complete irrigation infrastructure prevalence (mean pct_irrigated > 0.97) and confirmed hydrological coupling (ρ(SPEI-12, streamflow) = 0.75 and 0.82; ρ(streamflow, WUE) = 0.61 and 0.68). These basins concentrate Chile's export fruit and wine production under a regime where rights granted by the 1981 Water Code are permanent and freely tradeable, but where basin-scale reallocation cannot buffer a deficit that reduces supply for all rights holders simultaneously (Budds, 2020; Rivera et al., 2016). By contrast, Mataquito and Maule sub-watersheds show markedly lower mean sensitivities (0.12 and -0.03) despite similarly high irrigation prevalence (mean pct_irrigated 0.96 and 0.92), consistent with greater rainfall supplementation of snowmelt at higher latitudes. This north-to-south gradient implies that the lock-in risk of new perennial investment is not uniform across the Mediterranean zone: the same commitment to perennial horticulture or viticulture that carries moderate coupling risk in Maule carries substantially higher coupling risk in Aconcagua and Maipo, where meteorological drought and surface-water supply failure are most tightly linked. Under a sustained aridification trend, water-rights allocation frameworks that do not account for basin-level hydrological coupling may systematically underestimate the structural demand gap that long-horizon perennial commitments create.

These findings carry different implications depending on whether the management horizon is framed around transient drought or prolonged aridification. Contingency responses (groundwater banking, interbasin reallocation, reservoir buffering) cannot resolve structural exposure under directional aridification, because supplementary reserves are progressively depleted when below-normal conditions become the persistent baseline. Expanding snowmelt-dependent irrigation infrastructure or establishing new perennial orchards and vineyards during an ongoing aridification trend deepens crop-system lock-in, committing a watershed to inflexible water demand at precisely the timescale at which aridification operates. Conversely, annual-crop portfolio flexibility is associated with lower sensitivity and preserves capacity to adjust planted area during sustained supply deficits. WUE-based efficiency metrics are insufficient indicators of resilience under aridification: efficiency gains do not reduce supply coupling, and supply independence and crop-portfolio flexibility are the structural properties that differentiate lower-sensitivity from higher-sensitivity systems.

4.5. Methodological limitations and future directions

All findings are associative, derived from cross-sectional observational data. The paired-census quasi-experimental design provides evidence against drought-driven adaptive confounding but cannot establish that irrigation infrastructure is associated with heightened WUE sensitivity through a causal pathway. Findings

should be interpreted as structurally stable associations consistent with the proposed mechanisms.

Key limitations are: (i) the static agricultural mask may integrate natural vegetation patches, though matorral contamination was non-significant as a covariate and a barren-exclusion filter confirmed results (Supplementary Table S-7); (ii) the latitudinal gradient is the primary limitation for the irrigation result: adding centroid latitude attenuates the irrigation coefficient to non-significance (Table 1; Figure 8), while the annual-crops association strengthens, establishing it as the more latitude-robust result; (iii) *pct_irrigated* does not distinguish surface from groundwater irrigation, though DGA streamflow validation and aquifer co-decline evidence (Donoso, 2018) make groundwater confounding unlikely; (iv) spatial collinearity between irrigation and perennial crop share prevents isolation of a perennial-specific effect; non-significance of *pct_perennials* likely reflects collinearity rather than an absent pathway; (v) the CASEarth WUE dataset does not distribute component layers, so no formal NPP/ET attribution is presented; (vi) the 2007 census comparison is limited by imputation quality and is reported in Supplementary Table S-9 only; (vii) the cross-sectional design cannot establish the causal direction of the annual-crops association: the negative sign in 2021 (drought-sensitive watersheds have fewer annuals) is consistent with both structural buffering and drought-driven abandonment of annual cultivation; longitudinal data would allow discrimination between these mechanisms (Chakraborti et al., 2023; Xie et al., 2023).

5. Conclusions

Across 127 Chilean agricultural sub-watersheds (2001-2020), four principal conclusions emerge:

1. WUE decline is spatially concentrated in the central Mediterranean zone, co-located with NPP suppression (descriptive co-variation only). Negative trends and structural breaks both concentrate in the 30°S-35°S band.
2. SPEI and SPI carry practically equivalent cross-sectional information about WUE drought sensitivity (TOST equivalence $p<0.001$). Precipitation dominates the spatial gradient in WUE sensitivity at multi-year scales.
3. Annual crop share is robustly negatively associated with drought sensitivity across all latitude specifications (SEM $\beta = -0.322$ to -0.565, $p<0.01$). The negative sign is consistent with both structural buffering and drought-driven abandonment; causal direction cannot be established.
4. Irrigation infrastructure prevalence is positively associated with WUE-drought sensitivity in the full sample ($\beta=+0.422$, $p<0.001$), but this association attenuates substantially when latitude is controlled

(β=+0.109, p=0.327) and cannot be statistically isolated from the latitudinal aridity gradient. The evidence is consistent with demand-hardening theory but does not establish it.

Both crop-composition patterns are hypotheses warranting longitudinal validation. Neither can be treated as an established causal mechanism; effective governance under aridification requires explicit accounting for whether irrigation supply is genuinely decoupled from the same hydroclimatic signals that suppress crop productivity.

6. Funding

The National Research and Development Agency of Chile (ANID) funded this study through the drought emergency project FSEQ210022, Fondecyt Iniciación N°11190360, and Fondecyt Iniciación N°11230334. We declare that the authors have no competing interests, or other interests that might be perceived to influence the results and/or discussion reported in this paper.

7. Acknowledgements

The authors acknowledge the use of the CASEarth global cropland WUE dataset (Jiang et al., 2025), MODIS Terra products (MOD17A3HGF, MOD16A2GF) distributed by NASA Earthdata, CHIRPS v2.0 precipitation data and CHIRTS-daily temperature data provided by the Climate Hazards Center (University of California, Santa Barbara), and ERA5-Land reanalysis data provided by the European Centre for Medium-Range Weather Forecasts (ECMWF) via the Copernicus Climate Change Service (used for SWEI derivation). Agricultural census microdata were obtained from the Chilean Instituto Nacional de Estadísticas (INE). The authors declare no conflicts of interest.

8. Code and Data Availability

All analysis code is publicly available at https://github.com/frzambra/WUE_article (R scripts for all preprocessing, statistical analysis, and figure generation steps, with package versions managed via `renv` for reproducibility), enabling immediate reviewer access during manuscript evaluation. A permanent citable archive with a DOI will be deposited at Zenodo upon acceptance.

Annual cropland WUE rasters (NPP/ET, 1 km, 2001-2020) were obtained from Jiang et al. (2025), available at the CASEarth Data Platform (https://data.casearth.cn/dataset/640f0132819aec3f2b52a4bb). NPP data

(zNPP) were obtained from MOD17A3HGF (MODIS Terra, 500 m, Collection 6.1) for descriptive trend comparison only. ET anomaly data (SETI-12 December) were derived from MOD16A2GF (MODIS Terra, 500 m 8-day, Collection 6.1) for descriptive trend analysis only; no formal component attribution is presented as independent MODIS proxies do not algebraically reproduce the CASEarth WUE. For cross-product validation purposes, annual ET (zET) was additionally obtained from MOD16A3GF (MODIS Terra, 500 m annual, Collection 6.1; Supplementary Figure S-7). All MODIS products are available from NASA Earthdata (https://earthdata.nasa.gov). Drought index raster time series (SPEI, SPI, EDDI) were computed from CHIRPS v2.0 monthly precipitation (Funk et al., 2015) and CHIRTS-daily temperature (Funk et al., 2019), with SPEI and EDDI using FAO-56 Penman-Monteith reference evapotranspiration derived from CHIRTS. Snow Water Equivalent Index (SWEI) was derived from ERA5-Land monthly snow water equivalent reanalysis data. Agricultural census microdata for the 2007 and 2020-2021 censuses are publicly available from the Chilean Instituto Nacional de Estadísticas (INE; https://www.ine.gob.cl). Full software version details are listed in Section 2.6.

Declaration of generative AI and AI-assisted technologies in the manuscript preparation process

During the preparation of this work, the authors used Claude (Anthropic) to assist with the statistical analysis and to improve the English grammar. After using this tool, the authors reviewed and edited the content as needed and took full responsibility for the published article.

References

AghaKouchak, A., Farahmand, A., Melton, F.S., Teixeira, J., Anderson, M.C., Wardlow, B.D., Hain, C.R., 2015. Remote sensing of drought: Progress, challenges and opportunities. Reviews of Geophysics 53, 452–480. doi:10.1002/2014RG000456.

Barnett, T.P., Pierce, D.W., Hidalgo, H.G., Bonfils, C., Santer, B.D., Das, T., Bala, G., Wood, A.W., Nozawa, T., Mirin, A.A., et al., 2008. Human-induced changes in the hydrology of the western United States. Science 319, 1080–1083. doi:10.1126/science.1152538.

Bivand, R., Millo, G., Piras, G., 2021. A Review of Software for Spatial Econometrics in R. Mathematics 9, 1276. URL: https://www.mdpi.com/2227-7390/9/11/1276, doi:10.3390/math9111276.

Bivand, R., Wong, D.W.S., 2018. Comparing implementations of global and local indicators of spatial association. TEST 27, 716–748. doi:10.1007/s11749-018-0599-x.

Boisier, J., Alvarez-Garreton, C., Cordero, R., Damiani, A., Gallardo, L., Garreaud, R., Lambert, F., Ramallo, C., Rojas, M., Rondanelli, R., 2018. Anthropogenic drying in central-southern chile evidenced by long-term observations and climate model simulations. Elementa 6, 74. doi:10.1525/elementa.328.

Boser, A., Caylor, K., Larsen, A., Pascolini-Campbell, M., Reager, J., Carleton, T., 2024. Field-scale crop water consumption estimates reveal potential water savings in california agriculture. Nature Communications 15, 2366. doi:10.1038/s41467-024-46031-2.

Budds, J., 2020. Securing the market: Water security and the internal contradictions of chile's water code. Geoforum 113, 165–175. doi:10.1016/j.geoforum.2018.09.027.

Chakraborti, R., Davis, K.F., DeFries, R., Rao, N.D., Joseph, J., Ghosh, S., 2023. Crop switching for water sustainability in india's food bowl yields co-benefits for food security and farmers' profits. Nature Water 1, 864–878. doi:10.1038/s44221-023-00135-z.

Croissant, Y., Millo, G., 2008. Panel data econometrics in R: The plm package. Journal of Statistical Software 27, 1–43. doi:10.18637/jss.v027.i02.

Davis, K., Rulli, M., Seveso, A., D'Odorico, P., 2017. Increased food production and reduced water use through optimized crop distribution. Nature Geoscience 10, 919–924. doi:10.1038/s41561-017-0004-5.

Donoso, G. (Ed.), 2018. Water Policy in Chile. Springer International Publishing, Cham. doi:10.1007/978-3-319-76702-4. global Issues in Water Policy, Vol. 21.

Driscoll, J.C., Kraay, A.C., 1998. Consistent covariance matrix estimation with spatially dependent panel data. Review of Economics and Statistics 80, 549–560. doi:10.1162/003465398557825.

FAO y ONU Agua, 2025. Progreso del cambio en la eficiencia del uso del agua. doi:10.4060/cd2023es.

Fox, J., Weisberg, S., 2019. An R Companion to Applied Regression. 3 ed., Sage, Thousand Oaks, CA.

Funk, C., Peterson, P., Landsfeld, M., Pedreros, D., Verdin, J., Shukla, S., Husak, G., Rowland, J., Harrison, L., Hoell, A., et al., 2015. The climate hazards infrared precipitation with stations—a new environmental record for monitoring extremes. Scientific Data 2, 1–21. doi:10.1038/sdata.2015.66.

Funk, C., Peterson, P., Peterson, S., Shukla, S., Davenport, F., Michaelsen, J., Knapp, K.R., Landsfeld, M., Husak, G., Harrison, L., et al., 2019. A high-resolution 1983–2016 t_{max} climate data record based on infrared temperatures and stations by the climate hazard center. Journal of Climate 32, 5639–5658. doi:10.1175/JCLI-D-18-0698.1.

Garreaud, R., Boisier, J., Rondanelli, R., Montecinos, A., Sepúlveda, H., Veloso-Aguila, D., 2020. The central chile mega drought (2010–2018): A climate dynamics perspective. International Journal of Climatology 40, 421–439. doi:10.1002/joc.6219.

Gebrechorkos, S.H., Sheffield, J., Vicente-Serrano, S.M., Funk, C., Miralles, D.G., Peng, J., Dyer, E., Talib, J., Beck, H.E., Singer, M.B., Dadson, S.J., 2025. Warming accelerates global drought severity. Nature doi:10.1038/s41586-025-09047-2.

Grafton, R.Q., Williams, J., Perry, C.J., Molle, F., Ringler, C., Steduto, P., Udall, B., Wheeler, S.A., Wang, Y., Garrick, D., et al., 2018. The paradox of irrigation efficiency. Science 361, 748–750. doi:10.1126/science.aat9314.

Hellegers, P., Van Halsema, G., 2021. Sdg indicator 6.4.1 "change in water use efficiency over time": Methodological flaws and suggestions for improvement. Science of The Total Environment 801, 149431. doi:10.1016/j.scitotenv.2021.149431.

Hijmans, R.J., 2025. terra: Spatial Data Analysis. URL: https://CRAN.R-project.org/package=terra, doi:10.32614/CRAN.package.terra. r package version 1.8-54.

Hobbins, M.T., Wood, A., McEvoy, D.J., Huntington, J.L., Morton, C., Anderson, M., Hain, C., 2016. The evaporative demand drought index. part i: Linking drought evolution to variations in evaporative demand. Journal of Hydrometeorology 17, 1745–1761. doi:10.1175/JHM-D-15-0121.1.

Hoekstra, A., Mekonnen, M., 2012. The water footprint of humanity. Proceedings of the National Academy of Sciences 109, 3232–3237. doi:10.1073/pnas.1109936109.

Howden, S., Soussana, J.F., Tubiello, F., Chhetri, N., Dunlop, M., Meinke, H., 2007. Adapting agriculture to climate change. Proceedings of the National Academy of Sciences 104, 19691–19696. doi:10.1073/pnas.0701890104.

Hu, G., Jia, L., 2015. Monitoring of Evapotranspiration in a Semi-Arid Inland River Basin by Combining Microwave and Optical Remote Sensing Observations. Remote Sensing 7, 3056–3087. URL: https://www.mdpi.com/2072-4292/7/3/3056, doi:10.3390/rs70303056.

Immerzeel, W.W., Lutz, A.F., Andrade, M., Bahl, A., Biemans, H., Bolch, T., Hyde, S., Brumby, S., Davies, B.J., Elmore, A.C., et al., 2020. Importance and vulnerability of the world's water towers. Nature 577, 364–369. doi:10.1038/s41586-019-1822-y.

INE, 2007. VII Censo nacional agropecuario y forestal. Instituto Nacional de Estadística. Informe Agropecuarias 2007. Technical Report.

INE, 2021. VIII Censo Nacional Agropecuario y Forestal. Instituto Nacional de Estadísticas. Santiago, Chile. URL: https://www.ine.gob.cl/estadisticas-por-tema/agricultura-y-medio-ambiente/censo-agropecuario. resultados finales publicados en octubre de 2022.

Jiang, M., Zheng, C., Jia, L., Chen, J., 2025. A 20-year dataset (2001–2020) of global cropland water-use efficiency at 1-km grid resolution. Scientific Data 12, 574. doi:10.1038/s41597-025-04904-1.

Lutz, A.F., Immerzeel, W.W., Shrestha, A.B., Bierkens, M.F., 2014. Consistent increase in High Asia's runoff due to increasing glacier melt and precipitation. Nature Climate Change 4, 587–592. doi:10.1038/nclimate2237.

Malagueño, B.R., D'Odorico, P., 2024. ¿libre de la maleza estatista? Assessing neoliberal promises and water markets in Chile. Earth's Future doi:10.1029/2024EF004963.

McEvoy, D.J., Huntington, J.L., Hobbins, M.T., Wood, A., Morton, C., Anderson, M., Hain, C., 2016. The evaporative demand drought index. part ii: Conus-wide assessment against common drought indicators. Journal of Hydrometeorology 17, 1763–1779. doi:10.1175/JHM-D-15-0122.1.

Mckee, T.B., Doesken, N.J., Kleist, J., 1993. The relationship of drought frequency and duration to time scales, in: Proceedings of the Ninth Conference on Applied Climatology, American Metereological Society, Boston. pp. 179–184.

Paruelo, J.M., Texeira, M., Staiano, L., Mastrángelo, M., Amdan, L., Gallego, F., 2016. An integrative index of ecosystem services provision based on remotely sensed data. Ecological Indicators 71, 145–154. doi:10.1016/j.ecolind.2016.06.054.

Patakamuri, S.K., O'Brien, N., 2021. modifiedmk: Modified Versions of Mann Kendall and Spearman's Rho Trend Tests. URL: https://CRAN.R-project.org/package=modifiedmk, doi:10.32614/CRAN.package.modifiedmk. r package version 1.6.

Pebesma, E., 2018. Simple Features for R: Standardized Support for Spatial Vector Data. The R Journal 10, 439–446. URL: https://doi.org/10.32614/RJ-2018-009, doi:10.32614/RJ-2018-009.

Pebesma, E., Bivand, R., 2023. Spatial Data Science: With applications in R. Chapman and Hall/CRC. URL: https://r-spatial.org/book/, doi:10.1201/9780429459016.

584 Pedersen, T.L., 2025. patchwork: The Composer of Plots. URL: https://CRAN.R-project.org/package=
585 patchwork, doi:10.32614/CRAN.package.patchwork. r package version 1.3.1.

586 Pettitt, A.N., 1979. A non-parametric approach to the change-point problem. Journal of the Royal Statistical
587 Society: Series C (Applied Statistics) 28, 126–135. doi:10.2307/2346729.

588 Pohlert, T., 2023. trend: Non-Parametric Trend Tests and Change-Point Detection. URL: https://CRAN.R-
589 project.org/package=trend, doi:10.32614/CRAN.package.trend. r package version 1.1.6.

590 R Core Team, 2025. R: A Language and Environment for Statistical Computing. R Foundation for Statistical
591 Computing. Vienna, Austria. URL: https://www.R-project.org/.

592 Rivera, D., Godoy-Faúndez, A., Lillo, M., Alvez, A., Delgado, V., Gonzalo-Martín, C., Menasalvas, E.,
593 Costumero, R., García-Pedrero, Á., 2016. Legal disputes as a proxy for regional conflicts over water rights
594 in chile. Journal of Hydrology 535, 36–45. doi:10.1016/j.jhydrol.2016.01.057.

595 Running, S., Mu, Q., Zhao, M., Moreno, A., 2021. MODIS/Terra net evapotranspiration Gap-Filled 8-day
596 L4 global 500m SIN grid V061.

597 Tennekes, M., 2018. tmap: Thematic maps in R. Journal of Statistical Software 84, 1–39. doi:10.18637/
598 jss.v084.i06.

599 Vicente-Serrano, S.M., Beguería, S., López-Moreno, J.I., 2010. A multiscalar drought index sensitive to global
600 warming: The standardized precipitation evapotranspiration index. Journal of Climate 23, 1696–1718.
601 doi:10.1175/2009JCLI2909.1.

602 Wallace, J., 2000. Increasing agricultural water use efficiency to meet future food production. Agriculture,
603 Ecosystems & Environment 82, 105–119. URL: http://dx.doi.org/10.1016/S0167-8809(00)00220-6, doi:10.
604 1016/s0167-8809(00)00220-6.

605 Wang, T., Sun, S., Yin, Y., Zhao, J., Tang, Y., Wang, Y., Gao, F., Luan, X., 2024. Status of crop
606 water use efficiency evaluation methods: A review. Agricultural and Forest Meteorology 349, 109961.
607 doi:10.1016/j.agrformet.2024.109961.

608 Ward, F.A., Pulido-Velázquez, M., 2008. Water conservation in irrigation can increase water use. Proceedings
609 of the National Academy of Sciences 105, 18215–18220. doi:10.1073/pnas.0805554105.

610 Wickham, H., 2016. ggplot2: Elegant Graphics for Data Analysis. Springer-Verlag New York. URL:
611 https://ggplot2.tidyverse.org.

Wickham, H., Averick, M., Bryan, J., Chang, W., McGowan, L.D., François, R., Grolemund, G., Hayes, A., Henry, L., Hester, J., Kuhn, M., Pedersen, T.L., Miller, E., Bache, S.M., Müller, K., Ooms, J., Robinson, D., Seidel, D.P., Spinu, V., Takahashi, K., Vaughan, D., Wilke, C., Woo, K., Yutani, H., 2019. Welcome to the tidyverse. Journal of Open Source Software 4, 1686. doi:10.21105/joss.01686.

Xie, W., Zhu, A., Ali, T., Zhang, Z., Chen, X., Wu, F., Huang, J., Davis, K., 2023. Crop switching can enhance environmental sustainability and farmer incomes in china. Nature 616, 300–305. doi:10.1038/s41586-023-05799-x.

Yu, L., Gao, X., Zhao, X., 2020. Global synthesis of the impact of droughts on crops' water-use efficiency (WUE): Towards both high WUE and productivity. Agricultural Systems 177, 102723. URL: https://linkinghub.elsevier.com/retrieve/pii/S0308521X19301568, doi:10.1016/j.agsy.2019.102723.

Zambrano, F., Vrieling, A., Meza, F., Duran-Llacer, I., Fernández, F., Venegas-González, A., Raab, N., Craven, D., 2025. From Drought to Aridification: Land-Cover Fingerprints of a Drying Chile. Earth's Future 13, e2025EF006744. URL: https://agupubs.onlinelibrary.wiley.com/doi/10.1029/2025EF006744, doi:10.1029/2025EF006744.

Supplementary Material

Supplementary Table S-1 - Sample sizes by analytical step

Analysis	n	Spatial unit	Notes
WUE trend (Mann-Kendall)	127	Sub-watershed	Agricultural sub-watersheds with complete 2001-2020 WUE data
WUE-SPEI-12 sensitivity (OLS slope)	127	Sub-watershed	Same set; one per-sub-watershed regression per index
Pettitt change-point test	131	Sub-watershed	All sub-watersheds with a complete annual WUE series for the Pettitt test (4 more than the trend set, which additionally requires a valid prewhitened Mann-Kendall slope); 33.6% raw-significant change points reference this set
Panel regression (two-way FE)	131	Sub-watershed	Balanced panel; 131 × 20 = 2,620 sub-watershed-year obs.
Panel regression — Mediterranean subset	76	Sub-watershed	Mediterranean-climate sub-watersheds (Csa+Csb); panel N = 76 × 20 = 1,520 sub-watershed-year obs.

Analysis	n	Spatial unit	Notes
Crop composition OLS (2021 census)	127	Sub-watershed	Sub-watersheds with complete WUE, irrigation, and census data; three-predictor functional-aggregate specification
Crop composition spatial error model (2021)	127	Sub-watershed	Same set; `spatialreg::errorsarlm`, queen contiguity; λ = 0.468, $p < 0.001$
Crop composition OLS (2007 harmonized baseline)	127	Sub-watershed	2007 VII Census proportions; three-predictor functional-aggregate specification
Crop composition SEM (2007 baseline)	127	Sub-watershed	`spatialreg::errorsarlm`, queen contiguity; λ = 0.652, $p < 0.001$
Within-Csb crop composition (OLS + SEM)	67	Sub-watershed	Csb (warm-summer Mediterranean) subset; three-predictor functional-aggregate specification; OLS R^2 = 0.606, $F(3,63) = 32.2$, $p < 0.001$; SEM λ = 0.255, $p = 0.057$ (Supplementary Table S-4)

Analysis	n	Spatial unit	Notes
NPP and ET component sensitivity (zNPP-SPEI-12, SETI-12 Dec-SPEI-12)	143	Sub-watershed	Larger than 127: zNPP (MOD17A3HGF) and SETI-12 December (MOD16A2GF) are available for more sub-watersheds than the cropland-restricted Jiang WUE mask; n = sub-watersheds with complete MODIS sensitivity, irrigation, and census data

Supplementary Table S-2 - Köppen-stratified Wilcoxon signed-rank tests

Wilcoxon signed-rank tests comparing mean WUE in the pre-megadrought (2001-2009) versus megadrought (2010-2020) periods, stratified by Köppen climate class. Hodges-Lehmann median difference and 95% confidence interval are reported alongside p-values. Full numerical results are available in `outputs/tables/wilcox_by_climate_koppen.csv`.

Supplementary Table S-3 - Köppen-stratified panel regression (36-month indices)

Two-way fixed-effects panel regression coefficients for SPEI-36, SPI-36, and EDDI-36, estimated separately within each Köppen climate class with 5 sub-watersheds. Classes with $n < 5$ (Csa and extreme classes) were excluded. Full results for all nine indices (12/24/36-month) are in `outputs/tables/panel_regression_by_climate.csv`.

Köppen class	n sub-watersheds	Index		SE	p
BS (semi-arid)	14	SPEI-36	−0.307	0.213	0.150
BS	14	SPI-36	−0.079	0.190	0.679
BS	14	EDDI-36	−0.194	0.122	0.113
BW (arid)	8	SPEI-36	0.015	0.147	0.917

Köppen class	n sub-watersheds	Index		SE	p
BW	8	SPI-36	−0.168	0.123	0.176
BW	8	EDDI-36	0.190	0.123	0.123
Cf (humid-temperate)	26	SPEI-36	−0.287	0.088	**0.001**
Cf	26	SPI-36	−0.187	0.081	**0.022**
Cf	26	EDDI-36	−0.068	0.050	0.172
Csa (hot-summer Med.)	5	SPEI-36	0.085	0.280	0.763
Csa	5	SPI-36	0.263	0.216	0.228
Csa	5	EDDI-36	0.375	0.144	**0.011**
Csb (warm-summer Med.)	71	SPEI-24	0.180	0.062	**0.004**
Csb	71	SPEI-36	0.068	0.068	0.320
Csb	71	SPI-24	0.131	0.059	**0.026**
Csb	71	SPI-36	0.067	0.061	0.278
Csb	71	EDDI-36	−0.011	0.029	0.709

Bold p-values indicate significance at $p < 0.05$. The 24-month accumulation scale rows are included for Csb because SPEI-24 and SPI-24 show the strongest within-unit coupling in this class. Reference: `outputs/tables/panel_regression_by_climate.csv` and `outputs/tables/panel_cluster_robust_koppen.csv`.

Supplementary Table S-4 - Within-Csb crop-composition regression

Full version of Table 1 in Section 3.7. Crop-composition regression of WUE-SPEI-12 sensitivity restricted to warm-summer Mediterranean (Csb) sub-watersheds (n = 67), where the latitudinal aridity gradient is minimised, using the three-predictor functional-aggregate specification (reference category: forage/pasture). OLS $R^2 = 0.606$ ($F(3,63) = 32.2$, $p < 0.001$); SEM $= 0.255$ ($p = 0.057$). **Note on sample size:** Csb has 71 sub-watersheds in the panel regression (Supplementary Tables S-3, S-11); 4 are excluded from the within-Csb SEM because they lack complete irrigated-area data in the 2021 agricultural census, reducing the within-Csb SEM sample to n = 67.

Predictor	OLS	OLS SE	OLS p	SEM	SEM SE	SEM p
% Perennial crops	0.297	0.179	0.102	0.184	0.185	0.320
% Annual crops	−0.463	0.157	**0.004**	−0.565	0.173	**0.001**
% Irrigated area	0.317	0.128	**0.016**	0.264	0.137	0.053

The annual-crops effect is significant in both OLS and SEM within this single climate zone, confirming it as a crop-system property independent of the latitudinal gradient. Irrigation is significant in OLS but marginal in SEM (p = 0.053), consistent with the reduced spatial variation in irrigation access within the more homogeneous Csb zone. Perennial crop share is not significant within Csb, consistent with its status as a latitude-aridity co-variation artefact in the pooled model. Bold p-values indicate significance at $p < 0.05$. Reference: `outputs/tables/sensitivity_crop_within_csb.csv`.

Supplementary Table S-5 - WLS robustness check for the generated-regressor problem

Weighted least squares (WLS) regression of WUE-SPEI-12 sensitivity on 2021 functional crop group proportions (n = 127 sub-watersheds; reference category: forage/pasture), where each sub-watershed is weighted by the inverse squared standard error of its stage-1 sensitivity estimate ($1/SE^2$), down-weighting sub-watersheds whose WUE-SPEI-12 slopes are poorly constrained. Model fit: $R^2 = 0.712$, adj. $R^2 = 0.705$. Full results: `outputs/tables/sensitivity_crop_wls_regression.csv`.

Predictor	WLS	SE	95% CI	p
(Intercept)	−0.361	0.048	[−0.456, −0.266]	< 0.001
% Perennial crops	+0.501	0.115	[+0.274, +0.729]	< 0.001
% Annual crops	−0.265	0.080	[−0.423, −0.108]	0.001
% Irrigated area	+0.362	0.086	[+0.192, +0.533]	< 0.001

No sign changes relative to the primary OLS or SEM estimates: all three predictors retain direction and significance under stage-1 uncertainty weighting, confirming robustness to the generated-regressor design.

Perennial crops (WLS = +0.501) is stronger under WLS weighting, consistent with high-irrigation/perennial watersheds having more precisely estimated stage-1 slopes.

Supplementary Table S-6 - SWEI-based SEM (snowmelt robustness check)

Spatial error model (SEM) of WUE-SWEI sensitivity on 2021 functional crop group proportions (n = 127 sub-watersheds; reference category: forage/pasture; = 0.470, p < 0.001). Annual SWEI is defined as the August watershed-mean ERA5-Land SWE standardized using the EDDI procedure (Section 2.3.1). This model substitutes August peak SWEI for SPEI-12 as the drought index; the SPEI-12 SEM column reflects the updated CHIRPS/CHIRTS primary results (= 0.468). All three predictors preserve their sign relative to the SPEI-12 SEM. Full results are available in `outputs/tables/swei_sem_results.csv`.

Predictor	SPEI-12 SEM	SWEI SEM	95% CI (SWEI)	p (SWEI)	Sign consistent?
% Perennial crops	+0.219	+0.376*	[+0.055, +0.697]	0.022	Yes
% Annual crops	−0.322**	−0.139	[−0.447, +0.170]	0.378	Yes
% Irrigated area	+0.422***	+0.348*	[+0.080, +0.615]	0.011	Yes
(spatial error)	0.468***	0.470***	[+0.291, +0.648]	<0.001	—

* p < 0.05; ** p < 0.01; *** p < 0.001. Reference category: forage/pasture (*pct_forage*). Predictors are functional aggregates as defined in Section 2.4: perennial crops = fruits + vineyards; annual crops = cereals + vegetables + legumes + industrial crops. Median Spearman (SPEI-12, SWEI) across sub-watersheds = 0.296; in the top quartile of irrigated area share, median = 0.549.

Supplementary Table S-7 - Barren-exclusion dynamic mask robustness check

Crop-composition spatial error model (SEM) re-estimated after applying a barren-exclusion dynamic filter to address the static-mask / land-abandonment concern. For each year 2001–2020, pixels within the CASEarth "Cropland" static mask were additionally excluded where MODIS MCD12Q1.061 IGBP annual land-cover classified them as Barren (class 16), Urban (class 13), or Water bodies (class 17). Per-watershed

mean zWUE was re-extracted from the year-specific masked rasters, WUE-SPEI-12 sensitivity slopes were recomputed, and the three-predictor functional-aggregate SEM (reference category: forage/pasture) was refitted. The sample size was unchanged at n = 127 sub-watersheds. Full results are available in `outputs/tables/dynamic_mask_sem_comparison.csv`.

Predictor	Static-mask SEM	Barren-excl. SEM	95% CI (barren-excl.)	p (barren-excl.)	Sign consistent?
% Perennial crops	+0.219	+0.205	[−0.033, +0.443]	0.091	Yes
% Annual crops	−0.322**	−0.326**	[−0.550, −0.102]	**0.004**	Yes
% Irrigated area	+0.422***	+0.425***	[+0.228, +0.622]	**<0.001**	Yes
(spatial error)	0.468***	0.482***	[+0.302, +0.662]	**<0.001**	—

** $p < 0.01$; *** $p < 0.001$. All three substantive predictors are sign-consistent and statistically equivalent across both mask specifications, confirming that drought-driven land abandonment detectable as confirmed non-vegetation transitions in MODIS land cover does not materially alter the primary crop-composition findings.

Supplementary Table S-8 - Nonlinearity robustness check for post-2010 interaction

Two-way fixed-effects (within-unit) panel models for SPEI-36 testing whether the SPEI-36 × post-2010 interaction term captures non-linear physiological responses to severe drought rather than a genuine temporal structural break. M0 = linear baseline; M1 = adds quadratic SPEI² term; M2 = piecewise specification with extra slope for SPEI < 0; M3 = quadratic + post-2010 interaction. Full results are available in `outputs/tables/nonlinearity_panel_comparison.csv`.

Model	Term		SE_{std}	p_{std}
M0: linear	SPEI-36	−0.025	0.047	0.595
M1: +quadratic	SPEI-36	+0.109	0.057	0.054
M1: +quadratic	SPEI-36²	−0.131	0.032	**<0.001**

Model	Term		SE_{std}	p_{std}
M2: +piecewise	SPEI-36	−0.187	0.060	**0.002**
M2: +piecewise	SPEI-36 × I(SPEI < 0)	+0.509	0.117	**<0.001**
M3: quadratic+post-2010	SPEI-36	+0.329	0.152	**0.030**
M3: quadratic+post-2010	SPEI-36²	−0.218	0.064	**<0.001**
M3: quadratic+post-2010	SPEI-36 × post-2010	−0.312	0.200	0.119

All models: n = 131 sub-watersheds, 2,620 observations, two-way FE (unit + year). The M0 linear baseline is no longer significant (= −0.025, p = 0.595), consistent with the absence of a pooled within-unit SPEI-36 signal documented in Section 3.5. Nevertheless, M1 reveals a significant concave non-linear WUE-SPEI-36 relationship (SPEI-36² = −0.131, p < 0.001): the slope is steeper at negative SPEI values (drought conditions), as confirmed by the piecewise model M2 (SPEI-36 × I(SPEI < 0): = +0.509, p < 0.001). In M3, after controlling for this non-linearity, the post-2010 interaction is not significant (= −0.312, p = 0.119), indicating that the post-2010 intensification observed in the linear HC1 interaction model (Supplementary Figure S-6, = +0.281, p = 0.012) is largely attributable to the concentration of strongly negative SPEI-36 values in the 2010–2020 period operating on this concave response, rather than a discrete temporal structural break in the WUE-drought relationship.

Supplementary Table S-9 - Symmetric 2007 vs 2021 crop composition SEM comparison

The exact same three-predictor functional-aggregate specification (pct_perennials + pct_annuals + pct_irrigated, forage/pasture as reference category, spatial error model) applied to both the 2007 (pre-drought) and 2021 (post-drought) census data at n = 127 sub-watersheds. Only the census year differs, enabling a symmetric quasi-experimental test of whether the crop composition-WUE sensitivity

relationship is structural or an artefact of drought-driven adaptation. Full results are available in `outputs/tables/symmetric_census_comparison.csv`.

Predictor	2007 OLS	2007 SEM	95% CI (2007 SEM)	p (2007 SEM)	2021 SEM	95% CI (2021 SEM)	p (2021 SEM)	Sign consistent?
% Perennial crops	+0.386**	+0.016	[−0.195, +0.227]	0.885	+0.219	[−0.019, +0.456]	0.071	Yes
% Annual crops	−0.385**	−0.136	[−0.414, +0.142]	0.338	−0.322**	[−0.543, −0.101]	**0.004**	Yes
% Irrigated area	+0.476***	+0.467***	[+0.278, +0.657]	**<0.001**	+0.422***	[+0.226, +0.618]	**<0.001**	Yes
(spatial error)	—	0.652***	[+0.516, +0.788]	**<0.001**	0.468***	[+0.291, +0.645]	**<0.001**	—
n	127	127	—	—	127	—	—	—

** $p < 0.01$; *** $p < 0.001$. All three predictors are sign-consistent between census years. The irrigated area coefficient is sign-consistent and positive across both years (2007: = +0.467 vs 2021: = +0.422), a pattern consistent with structural stability; note that the 2007 value is partially imputed (Section 2.4) and direct quantitative comparison with the fully reported 2021 value is limited by imputation quality. Annual crops is sign-consistent but attenuated and non-significant in the 2007 SEM, partly reflecting stronger spatial autocorrelation (= 0.652 vs 0.468). Perennial crops is positive and sign-consistent in both SEM specifications but non-significant, consistent with the latitudinal confound (Section 4.5). Reference: `outputs/tables/symmetric_census_comparison.csv`.

Supplementary Table S-10 - Synchronized-time bootstrap two-stage uncertainty propagation

Bootstrap inference for the stage-2 spatial error model (SEM) of WUE-SPEI-12 sensitivity on 2021 crop composition (n = 127 sub-watersheds). Two bootstrap variants were implemented (code: `scripts/analysis/15_bootstrap_two_stage.R`; B = 1000 iterations each; seed = 2026):

Variant A — Pairs bootstrap (independent within-watershed): Each watershed draws its own random year indices. Captures within-watershed temporal sampling uncertainty but does not preserve the cross-sectional spatial covariance of stage-1 estimation errors.

Variant B — Synchronized-time bootstrap (primary): All 127 watersheds receive the SAME randomly drawn year indices in each iteration. Because the same calendar years are selected for all watersheds simultaneously, the spatial covariance of (SPEI-12, WUE) at each time point is preserved, and the resulting stage-1 slope estimates retain the cross-sectional spatial dependence present in the observed slopes (Moran's I = 0.514). Variant B is the primary inference reported here; Variant A is reported in `outputs/tables/bootstrap_comparison_variants.csv`.

Bootstrap 95% CIs are percentile intervals. Bootstrap p-values are two-sided: $2 \times \min(\text{proportion} \leq 0, \text{proportion} < 0)$. SE ratio = bootstrap SE / nominal SEM SE. Full results: `outputs/tables/bootstrap_two_stage_sem.csv`.

Predictor	Nominal	Nominal SE	Nominal p	Synced-time SE	Synced-time 95% CI	Synced-time p	SE ratio
(Intercept)	−0.275	0.062	< 0.001	0.094	[−0.421, −0.044]	0.018	1.511
% Perennial crops	+0.219	0.121	0.071	0.089	[+0.025, +0.363]	**0.032**	0.738
% Annual crops	−0.322	0.113	0.004	0.103	[−0.563, −0.142]	**0.002**	0.911
% Irrigated area	+0.422	0.100	< 0.001	0.078	[+0.229, +0.525]	**0.002**	0.776

The synchronized-time bootstrap produces SE ratios of 0.74–0.91× the nominal SEM SEs for the three substantive predictors, notably more conservative than the pairs bootstrap (0.53–0.76×). All three predictors remain significant under the spatially-correct bootstrap (p = 0.002–0.032). Compare Supplementary Table S-5 (WLS robustness check) for the complementary inverse-variance weighting approach; full variant comparison in `outputs/tables/bootstrap_comparison_variants.csv`.

Supplementary Table S-11 - Complete within-unit panel regression: HC1 vs Driscoll-Kraay standard errors

Two-way fixed-effects panel regression coefficients for all nine index × accumulation-scale combinations, estimated in the full study domain (n = 131 sub-watersheds, 2,620 obs.) and restricted to Mediterranean-climate sub-watersheds (Csa+Csb, n = 76, 1,520 obs.). **Two SE variants are reported:** HC1 (clustered by sub-watershed, accounts for within-unit serial correlation only; assumes cross-sectional independence) and Driscoll-Kraay (DK; Driscoll and Kraay (1998), bandwidth = $\lfloor T^{1/4} \rfloor = 2$, accounts for both serial correlation AND cross-sectional spatial dependence). The DK estimator is the methodologically appropriate choice given Moran's I = 0.514–0.683 for WUE-SPEI slopes. Bold p-values indicate $p < 0.05$ under DK SEs. Full results: `outputs/tables/panel_driscoll_kraay.csv` (DK primary) and `outputs/tables/panel_cluster_robust.csv` (HC1 for reference).

Index	Scale		HC1 SE	HC1 p	**DK SE**	**DK p**	DK ratio
SPEI	12	−0.112	0.034	0.001	0.102	0.273	3.0×
SPEI	24	+0.046	0.046	0.316	0.156	0.769	3.4×
SPEI	36	−0.025	0.042	0.553	0.146	0.879	3.5×
SPI	12	−0.170	0.027	<0.001	0.087	0.053	3.2×
SPI	24	+0.001	0.037	0.968	0.139	0.994	3.8×
SPI	36	−0.026	0.040	0.513	0.156	0.870	3.9×
EDDI	12	−0.009	0.019	0.633	0.056	0.873	3.0×
EDDI	24	−0.021	0.024	0.377	0.074	0.778	3.1×
EDDI	36	−0.036	0.026	0.178	0.086	0.682	3.3×

All watershed panel (n = 131). None of the nine indices reach DK significance at any accumulation scale. HC1 p-values for SPEI-12 (0.001) and SPI-12 (<0.001) reflect within-unit serial correlation corrections that do not account for the strong cross-sectional spatial dependence.

Index	Scale	(Med.)	HC1 SE	HC1 p	**DK SE**	**DK p**
SPEI	24	+0.193	0.046	<0.001	0.259	0.458
SPI	24	+0.141	0.041	0.001	0.254	0.579
SPEI	12	+0.080	0.051	0.102	0.132	0.555
SPI	12	−0.025	0.045	0.576	0.119	0.963

Index	Scale	(Med.)	HC1 SE	HC1 p	**DK SE**	**DK p**
SPEI	36	+0.082	0.047	0.079	0.170	0.630

Mediterranean subset (n = 76). All coefficients are non-significant under DK SEs. Because the DK correction renders these estimates statistically indistinguishable from zero, their signs cannot be reliably interpreted as physical signals; the panel provides no statistically reliable evidence for within-unit temporal coupling in this subset.

Several patterns are noteworthy. First, SPEI-12 and SPI-12 are significantly negative in the full panel ($p = 0.001$ and $p < 0.001$, respectively). This is a heterogeneity average: humid-temperate Cf sub-watersheds (n = 26) exhibit strong negative within-unit coupling (SPEI-36 $= -0.287$; Supplementary Table S-3), where rainfed annual systems raise WUE under mild drought by suppressing ET more than NPP (Yu et al., 2020). Removing Cf watersheds and restricting to Mediterranean (Csa+Csb) reverses the 12-month sign and reveals positive within-unit coupling at 24 months. Second, within Mediterranean sub-watersheds, EDDI-12 ($= -0.064$, $p = 0.009$) and EDDI-24 ($= -0.079$, $p = 0.010$) are negative in the cluster-robust panel analysis. All EDDI values reported in this table use the manuscript's sign convention (positive = below-normal demand; negative = drought, inverted from Hobbins et al. (2016); Section 2.3.1). Under this convention, a negative within-unit EDDI coefficient means years with below-normal evaporative demand are associated with lower WUE within Mediterranean watersheds, a result consistent with irrigated perennial systems sustaining higher actual ET in mild-demand years without a proportional NPP gain, reducing the NPP/ET ratio. The EDDI within-unit finding is not central to any primary manuscript conclusion; SPEI-12 and SPI-12 are the main cross-product validated indices, and EDDI results are reported for completeness. Third, neither SPEI nor SPI shows significant within-unit coupling at the 36-month scale in any subset, and only the 24-month Mediterranean results are clearly positive and consistent across both precipitation-based indices.

Supplementary Table S-12 - Cross-sectional variance partition: contextual analysis with dimensional caveat

Important methodological caveat (see ?@sec-acummulation-scale_selection_and_cross-sectional_context): Drought indices (SPEI-12, SPI-12) are standardized temporal anomalies relative to each watershed's local historical mean; they contain very little information about the absolute spatial aridity gradient at a single time point. WUE in 2020 and crop composition both co-vary with the spatial climatology (latitudinal aridity gradient). The near-zero unique cross-sectional variance attributable to

drought indices is therefore a dimensional artifact: SPEI/SPI have been standardized to remove the same spatial gradient that drives both WUE and crop composition. **This table should not be interpreted as showing that drought is less important than crop composition for explaining WUE.** The table is retained for transparency and to document why adding drought indices to the cross-sectional model produces negligible R^2 gain. Full results: `outputs/tables/r2_variance_partition.csv`.

Variance partition of the 2020 cross-sectional regression of zWUE on drought index and crop composition (n = 131 sub-watersheds). Crop proportions: pct_frutales, pct_vides, pct_cereales, pct_hortalizas, pct_forrajeras_y_praderas.

Index	R^2 (index only)	R^2 (crops only)	R^2 (full)	Unique to index	Shared	Unique to crops
SPEI-12	0.100	0.436	0.451	0.015	0.085	0.351
SPI-12	0.005	0.436	0.438	0.002	0.003	0.432
EDDI-24	0.213	0.436	0.454	0.018	0.196	0.240

The near-zero unique drought-index variance (SPEI-12 = 0.015; SPI-12 = 0.002) is a consequence of standardization: SPEI removes the spatial mean, leaving only the 2020 temporal anomaly, which explains little of the spatial variance that both WUE and crop composition carry through the absolute aridity gradient. The larger unique contribution of EDDI-24 (0.018) and its higher shared variance with crops (0.196) reflects evaporative demand's stronger spatial structure; even here, the dimensional limitation applies.

Supplementary Table S-13 - DGA streamflow validation: delivery co-variation in key irrigation basins

Panel A — Cuenca-level delivery validation (primary analysis). Cross-product correlations between CHIRPS/CHIRTS SPEI-12 (December, cuenca mean across study sub-watersheds) and DGA annual streamflow anomaly (all gauges within each cuenca; calendar-year mean, standardised) for five key irrigation basins over 2001–2019 (n = 19 years each; data: CR2 `cr2_qflxDaily_2020`; code: `scripts/analysis/18b_dga_delivery_validation_mediterranean.R`; full results: `outputs/tables/delivery_validat`

Cuenca	n gauges	(SPEI-12, Q_annual)	(Q_annual, WUE)	(SPEI-12, WUE)
Aconcagua (054)	14	**0.746**	**0.614**	0.560
Maipo (057)	25	**0.816**	**0.684**	0.763

Cuenca	n gauges	(SPEI-12, Q_annual)	(Q_annual, WUE)	(SPEI-12, WUE)
Rapel (060)	19	**0.723**	**0.384**	0.461
Mataquito (071)	7	**0.828**	0.289	0.033
Maule (073)	46	**0.809**	−0.198	−0.160
Median	—	**0.809**	**0.384**	0.461

All five basins show (SPEI-12, Q_annual) 0.72 (all positive and strong): drought years (lower SPEI-12) consistently delivered lower annual streamflow. WUE was positively correlated with streamflow in the three northern irrigation basins (Aconcagua, Maipo, Rapel), confirming the SPEI to streamflow to WUE co-variation chain. Mataquito and Maule show weaker WUE-streamflow coupling consistent with their transitional hydroclimatic position toward the humid-temperate zone. All correlations are fully cross-product (CHIRPS/CHIRTS SPEI vs. independently observed DGA streamflow) with no shared forcing.

Panel B — Sub-watershed-level analysis (supporting). Sub-watershed analysis using only gauges that fall inside the DGA sub-watershed polygons (n = 16 sub-watersheds, Cf-dominated): median (SPEI-12, Q) = 0.57 (range 0.13–0.78). Sub-watershed coverage is geographically biased toward the humid-temperate Cf zone; the cuenca-level analysis (Panel A) is the primary validation. Full results: `outputs/tables/streamflow_spei_wue_correlations.csv`.

Supplementary Figure S-1 - Pre-drought (2007) crop composition and WUE sensitivity

Supplementary Figure S-2 - Mean WUE-drought correlation by index, accumulation scale, and Köppen class

Supplementary Figure S-3 - Natural-vegetation covariate robustness

Supplementary Figure S-4 - Geographic (latitude-block) cross-validation

This figure has been moved to the main text as Figure 8 (in Section 4.4). All five latitude-block holdout R^2 values are negative (range −1.56 to −0.30); full cross-validation results are in `outputs/tables/spatial_cv_by_block.csv`.

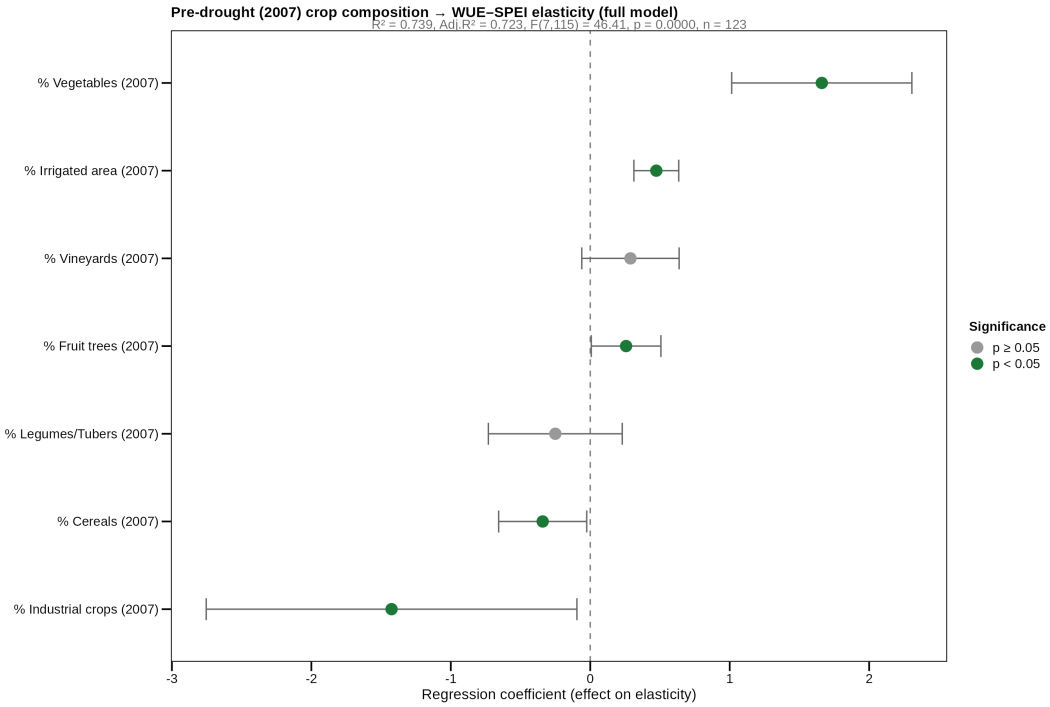

Figure 9: Pre-drought (2007) crop composition as a predictor of WUE-SPEI-12 sensitivity. OLS and spatial error model (SEM) regression coefficient plots using VII Agricultural and Forestry Census (2007) individual-category proportions aggregated to sub-watershed level as predictors (reference category: forage/pasture; n = 127 sub-watersheds). The harmonized OLS uses a five-predictor individual-category specification; the SEM uses the full seven-predictor specification (including legumes/tubers and industrial crops). Only the irrigated area coefficient is significant in the 2007 SEM (= +0.467, $p < 0.001$), consistent with irrigation amplification being a pre-drought structural property, though the 2007 imputation (Section 2.4) limits the reliability of this comparison with the 2021 result. The cereal (annual-crops proxy) coefficient is directionally consistent with the 2021 result in OLS but not significant in the 2007 SEM; the 2007 and 2021 CIs overlap substantially and no formal test of coefficient difference has been conducted. Reference: `outputs/tables/elasticity_crop_2007_regression.csv`.

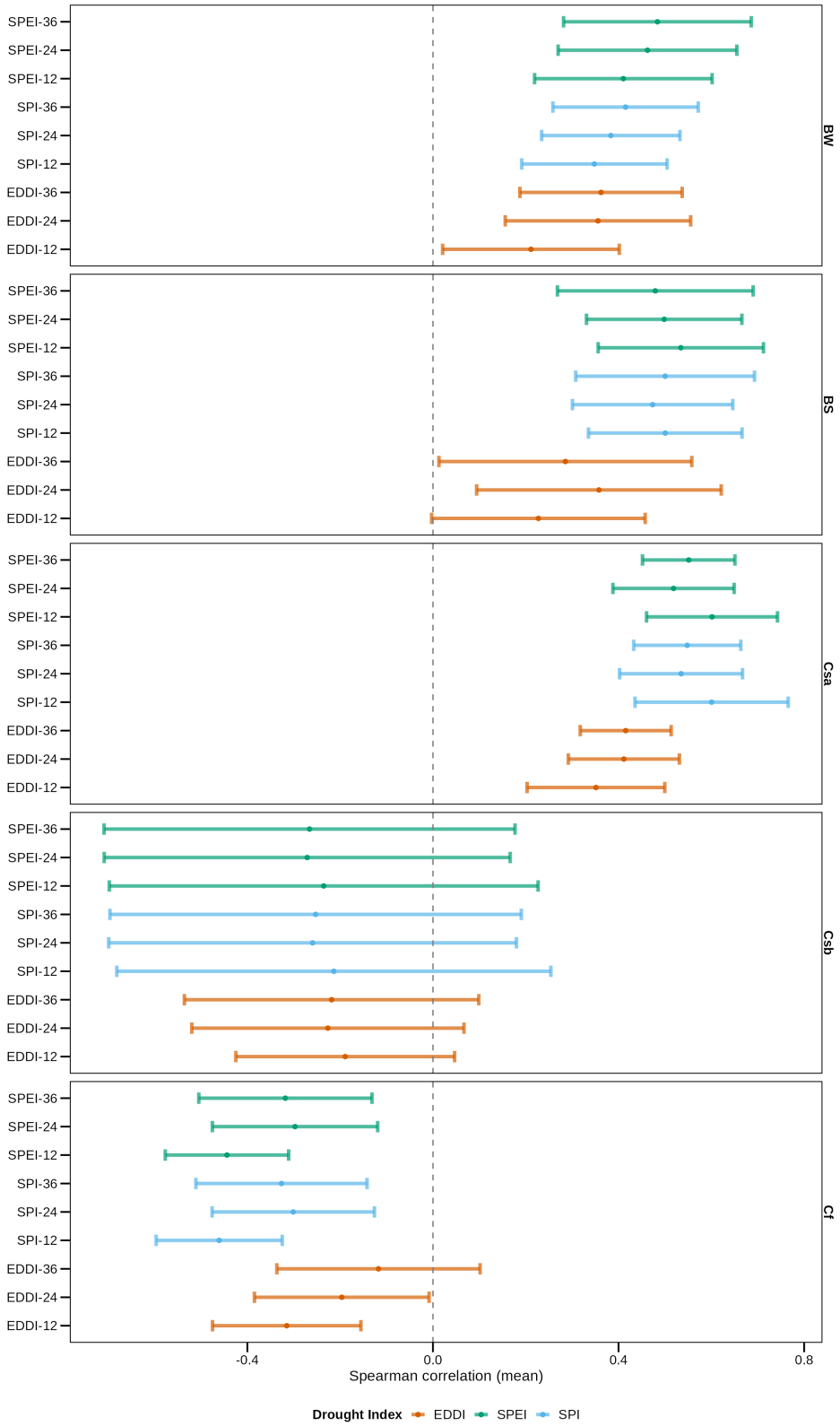

Figure 10: Mean per-sub-watershed Spearman correlation between annual WUE and each drought index (SPEI, SPI, EDDI) at the 12-, 24-, and 36-month accumulation scales, stratified by Köppen climate class. Points show the across-sub-watershed mean correlation; horizontal bars show the spread. This figure is the evidence base for foregrounding the 36-month accumulation scale and for the conclusion that SPEI and SPI carry comparable information while EDDI is weaker; it also exposes the Cf (humid-temperate) sign reversal that the panel regression formalizes.

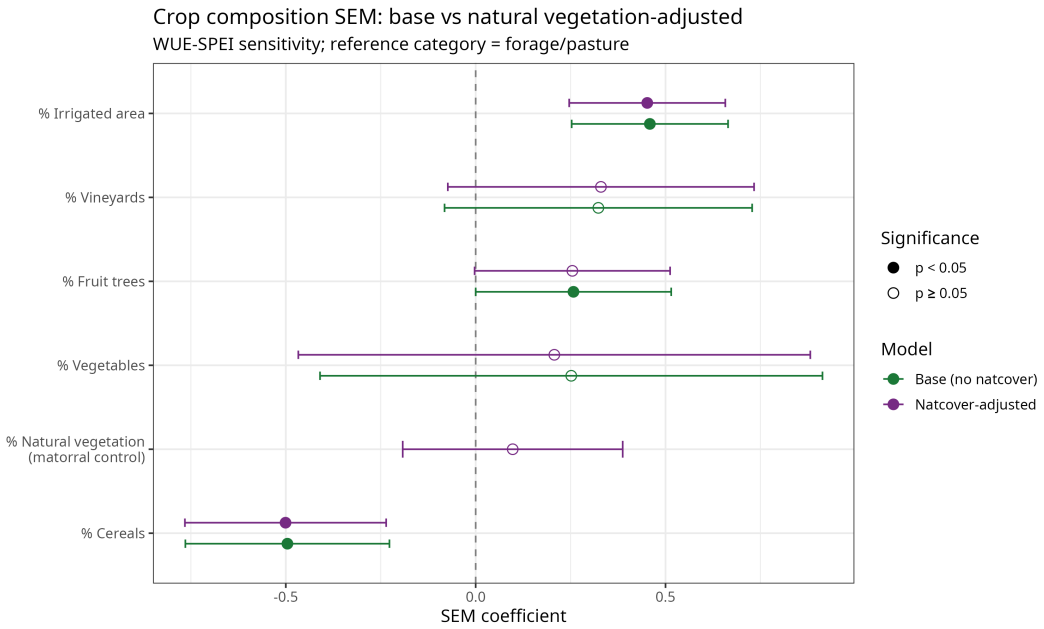

Figure 11: Robustness of the crop composition-WUE-SPEI-12 sensitivity associations to natural-vegetation (matorral) contamination within the agricultural mask. Spatial error model coefficients are compared between the base specification (green) and a specification that adds the natural-vegetation fraction (ESA CCI-LC 2016) as a control covariate (purple; reference category: forage/pasture). Solid symbols denote $p < 0.05$. The natural-vegetation coefficient is non-significant ($= 0.098$, $p = 0.509$) and the cereal (negative) and irrigated-area (positive) effects are essentially unchanged, indicating that matorral fragmentation does not confound the crop composition-sensitivity relationship.

Supplementary Figure S-5 - Köppen-stratified panel regression coefficients

Supplementary Figure S-6 - Panel regression: pooled, Mediterranean, and post-2010 intensification

Supplementary Figure S-7 - Cross-product uncertainty analysis

Supplementary Table S-14 - Latitude-control robustness check for the irrigation effect

Spatial error model (SEM) of WUE-SPEI-12 sensitivity on 2021 functional crop group proportions (n = 127 sub-watersheds; reference category: forage/pasture), estimated under three specifications: M0 = primary model without latitude (replicates Table 1 full-sample SEM); M1 = adds sub-watershed centroid latitude (°S, negative values); M2 = adds centroid latitude and latitude². The Standardized Snow Water Equivalent Index (SWEI) procedure is defined in Section 2.3.1. Results address the reviewer concern that the irrigation association may be confounded with the latitudinal aridity gradient. Spatial weights: queen contiguity. Full results: `outputs/tables/latitude_control_sem_comparison.csv`.

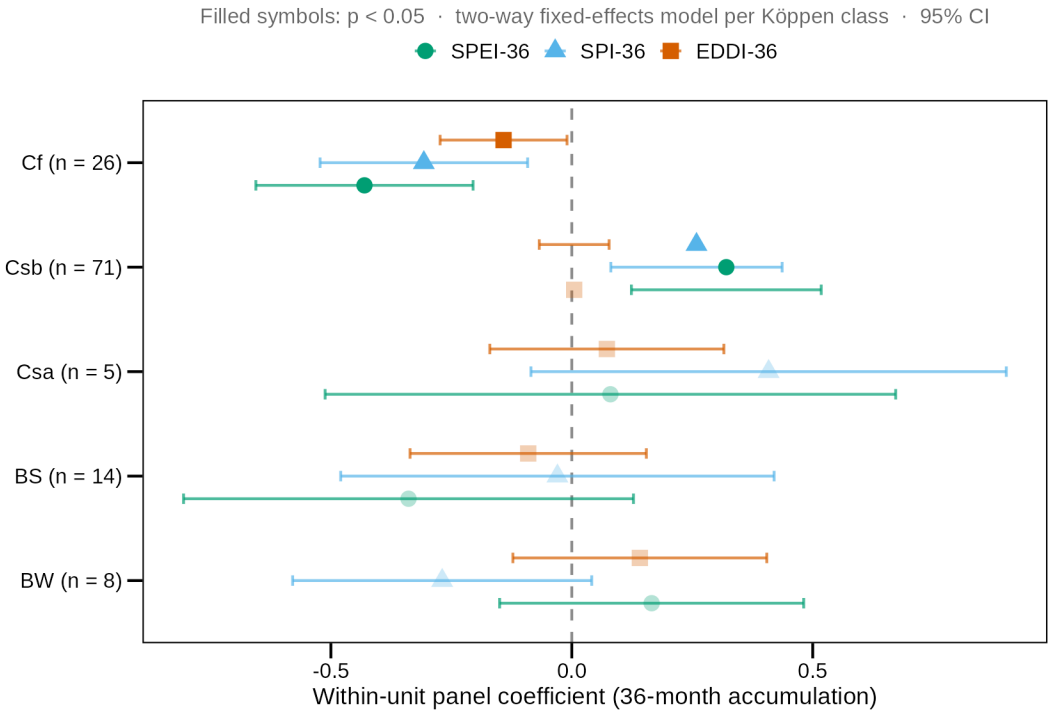

Figure 12: Two-way fixed-effects panel regression coefficients at the 36-month accumulation scale (SPEI-36, SPI-36, EDDI-36), estimated separately within each Köppen climate class (visualizing Supplementary Table S-3). Points show the within-unit coefficient with 95% confidence intervals; filled symbols denote $p < 0.05$. The figure makes explicit the divergence between Csb (warm-summer Mediterranean) sub-watersheds, which show significant positive WUE-drought coupling, and Cf (humid-temperate) sub-watersheds, which show a significant negative sign reversal at the 36-month scale; arid and semi-arid classes (BW, BS) show no significant within-unit coupling.

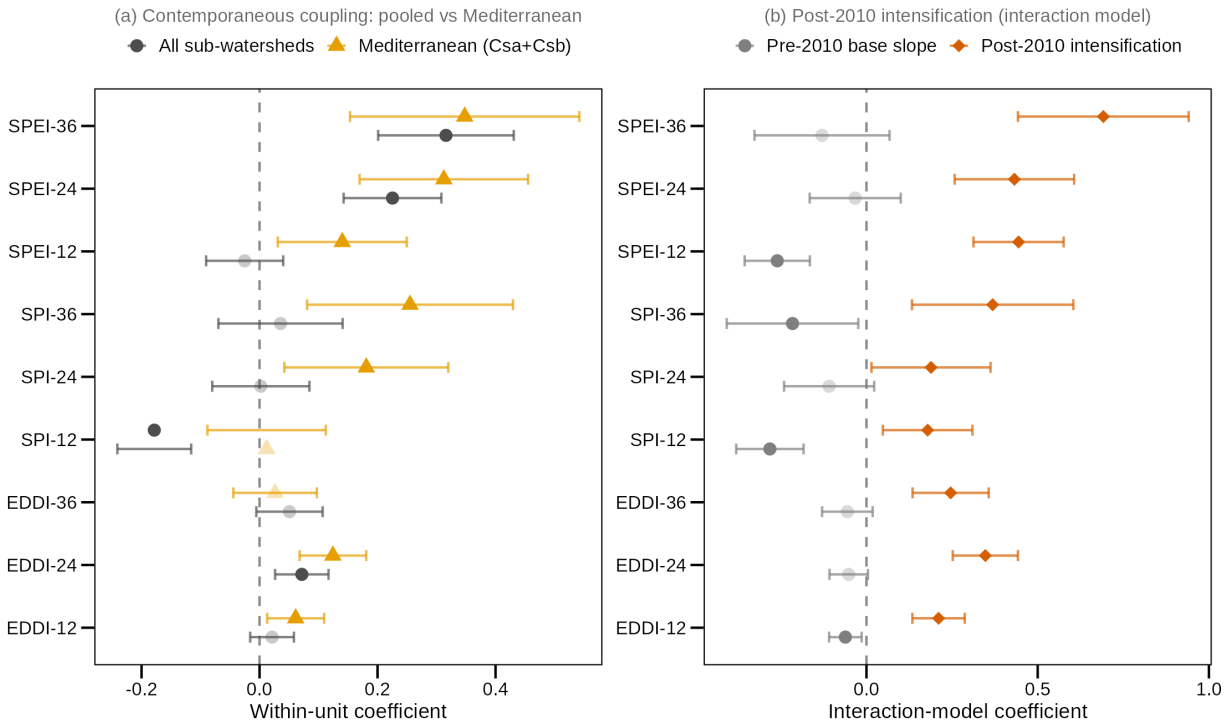

Figure 13: Two-way fixed-effects panel regression coefficients with 95% confidence intervals; filled symbols denote $p < 0.05$. (a) Contemporaneous within-unit WUE-drought coupling for SPEI, SPI, and EDDI at the 12-, 24-, and 36-month accumulation scales, comparing all sub-watersheds (grey) with the Mediterranean subset (Csa+Csb, orange). SPEI-24 and SPI-24 couple significantly within Mediterranean sub-watersheds; 36-month indices are non-significant in the all-watershed panel. (b) Interaction model contrasting the pre-2010 base slope (grey) with the post-2010 intensification term (vermillion). The post-2010 term is significant and positive for all three indices at the 36-month scale under HC1 standard errors (SPEI-36 post-2010 $= +0.281$, $p = 0.012$); this result does not survive Driscoll-Kraay correction and is explained by concave nonlinearity rather than a structural break (Supplementary Table S-8).

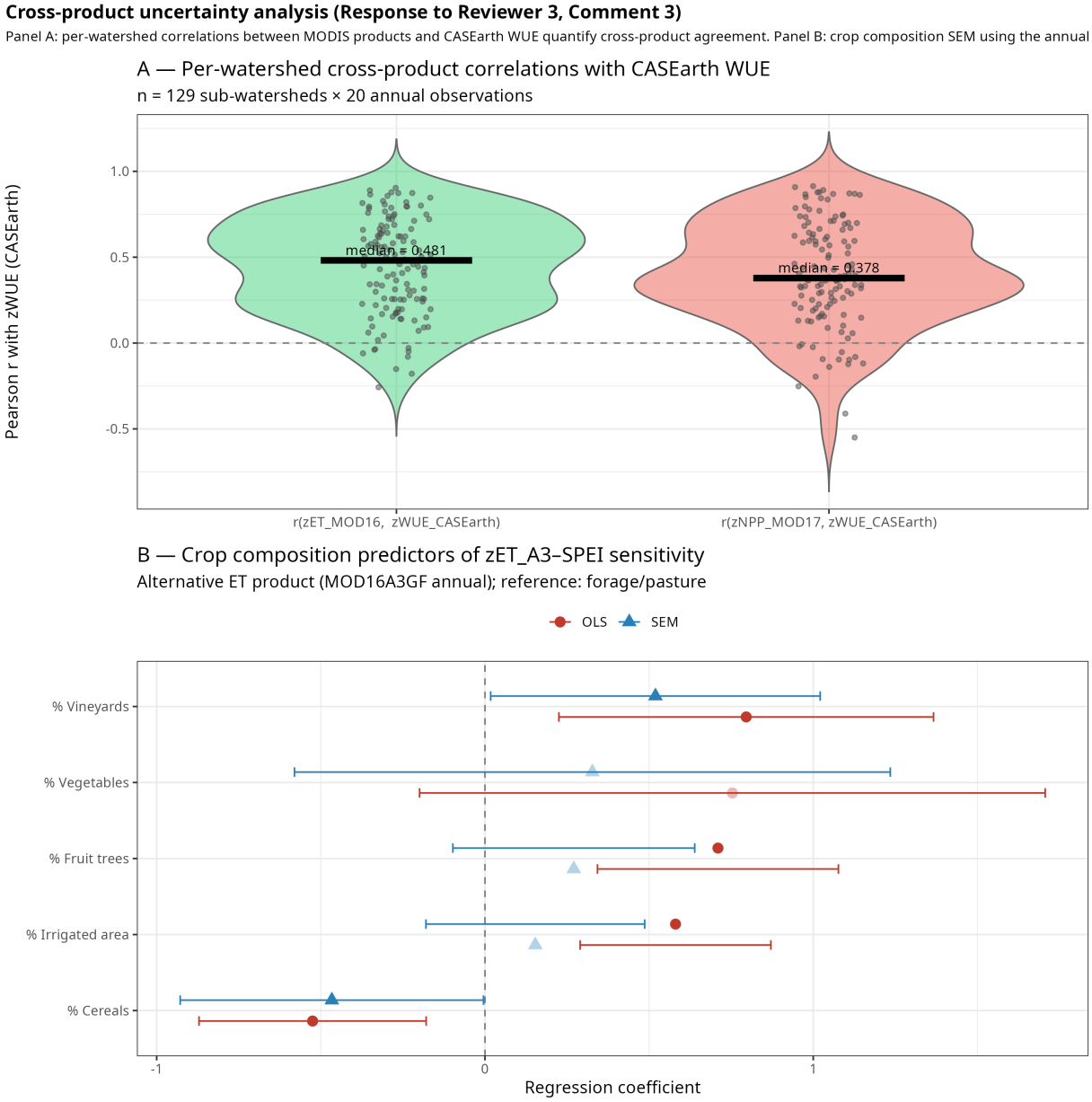

Figure 14: Cross-product uncertainty analysis for the WUE component sensitivity comparison (response to cross-product inconsistency concern, Section 2.3.2). Panel A: distributions of per-watershed Pearson correlations between each MODIS product and CASEarth zWUE (n = 129 sub-watersheds × 20 years). Median r(zNPP_MOD17, zWUE_CASEarth) = 0.378 and r(zET_MOD16, zWUE_CASEarth) = 0.481 are not significantly different (Wilcoxon paired test p = 0.272), confirming both products capture real WUE-relevant signals comparably. Panel B: crop-composition regression coefficients for the alternative annual ET product (MOD16A3GF; zET-SPEI-12 sensitivity), showing OLS (red circles) and SEM (blue triangles) estimates with 95% CI. Vineyard proportion is a significant positive predictor in SEM (= 0.519, p = 0.043), confirming that the NPP-channel vineyard association is not a MODIS cross-product artefact.

Predictor	M0 (no lat)	M0 p	M1 (+ lat)	M1 p	M2 (+ lat²)	M2 p
% Perennial crops	+0.219	0.071	+0.025	0.833	+0.020	0.866
% Annual crops	−0.322	0.004	−0.485	<0.001	−0.440	<0.001
% Irrigated area	+0.422	<0.001	+0.109	0.327	+0.116	0.290
Latitude (centroid)	—	—	+0.062	<0.001	+0.218	0.097
Latitude²	—	—	—	—	+0.002	0.232
AIC	−39.0		−59.4		−58.8	

When latitude is explicitly controlled (M1), the irrigation coefficient attenuates from = +0.422 to = +0.109 and loses significance (p = 0.327), while latitude is highly significant (= +0.062, p < 0.001). Model fit improves markedly (ΔAIC = 20.4), confirming that latitude captures substantial variance in WUE sensitivity. The annual-crops buffering effect strengthens under latitude control (M0: = −0.322 → M1: = −0.485) and remains significant, establishing it as the more robustly latitude-independent result. The quadratic latitude term (M2) is non-significant (p = 0.232), indicating the latitudinal gradient is approximately linear over the study domain. Residual Moran's I is non-significant in all three models (p > 0.70), confirming adequate spatial error correction.